Article

Optimal Modeling and Feasibility Analysis of Grid-Interfaced Solar PV/Wind/Pumped Hydro Energy Storage Based Hybrid System

Isaac Amoussou [1][ID], Emmanuel Tanyi [1], Ahmed Ali [2,*], Takele Ferede Agajie [1][ID], Baseem Khan [3,4,*][ID], Julien Brito Ballester [4,5] and Wirnkar Basil Nsanyuy [1]

1   Department of Electrical and Electronic Engineering, Faculty of Engineering and Technology, University of Buea, Buea P.O. Box 63, Cameroon
2   Department of Electrical and Electronic Engineering Technology, Faculty of Engineering and the Built Environment, University of Johannesburg, Cnr Kingsway & University Roads, Auckland Park, P.O. Box 524, Johannesburg 2092, South Africa
3   Department of Electrical and Computer Engineering, Hawassa University, Hawassa P.O. Box 05, Ethiopia
4   Department of Project Management, Universidad Internacional Iberoamericana, Campeche 24560, Mexico
5   Department of Project Management, Universidad Europea del Atlántico, C/Isabel Torres 21, 39011 Santander, Spain
*   Correspondence: aali@uj.ac.za (A.A.); baseem.khan04@ieee.org (B.K.)

Abstract: Access to inexpensive, clean energy is a key factor in a country's ability to grow sustainably The production of electricity using fossil fuels contributes significantly to global warming and is becoming less and less profitable nowadays. This work therefore proposes to study the different possible scenarios for the replacement of light fuel oil (LFO) thermal power plants connected to the electrical network in northern Cameroon by renewable energy plants. Several scenarios such as the combination of solar photovoltaic (PV) with a pumped hydro storage system (PHSS), Wind and PHSS and PV-Wind-PHSS have been studied. The selected scenarios are evaluated based on two factors such as the system's total cost (TC) and the loss of load probability (LOLP). To achieve the results, metaheuristics such the non-dominated sorting whale optimization algorithm (NSWOA) and non-dominated sorting genetic algorithm-II (NSGA-II) have been applied under MATLAB software. The optimal sizing of the components was done using hourly meteorological data and the hourly power generated by the thermal power plants connected to the electrical grid. Both algorithms provided satisfactory results. However, the total cost in the PV-PHSS, Wind-PHSS, and PV-Wind-PHSS scenarios with NSWOA is, respectively, 1%, 6%, and 0.2% lower than with NSGA-II. According to NSWOA results, the total cost for the PV-Wind-PHSS scenario at LOLP 0% is 4.6% and 17% less than the Wind-PHS and PV-PHSS scenarios, respectively. The profitability study of all three scenarios showed that the project is profitable regardless of the scenario considered.

Keywords: thermal power plants; wind; PV; LOLP; NSWOA; NSGA-II PHS; renewable energy; total cost

1. Introduction

Fossil fuel use within the energy sector has compelled human cultures to reconsider their way of life in order to lessen the quantity of greenhouse gases released into the atmosphere. The power and heat generation sectors account for 46% of the increase in greenhouse gas emissions in the environment in 2021 [1]. With the unprecedented increase in the price of fossil fuels such as gas and diesel, most countries in the world are planning and accelerating the transition from fossil fuels to cleaner and more environmentally friendly renewable energy sources. In turn, fossil fuels are becoming increasingly scarce and depleted. Some studies have predicted the total depletion of fossil energy sources to take place within a few decades [2]. In this context, alternative sources of green energy

such as solar and wind power are set to take a larger share in the energy mix of the world's countries. Additionally, the technologies used in the design of the various components of solar and wind systems are increasingly mature [3,4] and affordable [5]. However, due to the intermittency of these two energy sources related to weather conditions, their use as a replacement for conventional energy sources poses some challenges. Indeed, the production of energy from intermittent energy sources can cause a mismatch between demand and production. Similarly, renewable energy sources sometimes cause stability problems when connected to power grids. To overcome these problems, energy storage systems are associated with variable renewable energy production systems. The storage systems ensure the continuity of the energy supply to the different consumers even in case of a sudden variation of the renewable energy production systems. Among the existing types of energy storage systems, the most widely used is pumped hydro storage systems [6,7] since they have long life spans and a minimal cost of energy as compared to battery and thermal energy storage systems [8,9]. The total installed PHS capacity reached 127 GW and represented more than 99% of the total installed storage capacity worldwide [10]. The maturity, energy cost and especially the lifetime of PHS are their fundamental advantages compared to other types of storage. Nevertheless, the installation of large-scale PHS systems requires favorable topographical conditions [11] and the availability of water resources [12].

The integration of storage systems in renewable energy conversion systems has a considerable impact on the total cost of the projects and on the cost of energy conversion. The issue of having an optimal size begins to emerge. In the literature, several optimization strategies are utilized to optimally size hybrid renewable energy systems, for instance, through the use of software such as HOMER and meta-heuristic algorithms. The optimal sizing of renewable energy systems is frequently carried out using meta-heuristics based on economic criteria such as life cycle cost (LCC) [13], cost of energy (COE) [14,15], net present cost (NPC) [16,17], and technical reliability criteria such as loss of load probability (LOLP) [18,19], loss of load expected (LOLE) [20], and loss of power supply probability (LPSP) [21,22]. A number of research studies have investigated the appropriate size of grid-connected renewable energy systems using meta-heuristic algorithms in accordance with economic and technical criteria. Thus, in [23], the author proposed three algorithms; the whale optimization algorithm (WOA), particle swarm optimization (PSO), and fire fly were used to minimize the cost of energy (COE) and the probability of a power supply disruption. The COE of the pumped-hydro storage hybrid system was determined to be lower (0.215 $/kWh) than that of the battery storage hybrid system (0.254 $/kWh), which was derived using WOA at the same load demand. A study employing the modified crow search algorithm (CSA) to reduce fuel usage in a PV/diesel/PHS stand-alone system was published in [24]. The results obtained with the modified CSA were compared with the results obtained using a genetic algorithm (GA) and PSO. It was found that the results obtained using modified CSA are better than those obtained using GA and PSO. The optimal sizing of a hybrid solar PV, biogas and PHS system isolated from the electrical grid can be done with the help of metaheuristics such as water cycle algorithm (WCA), Moth flame optimization (MFO) and GA following the total net present cost (TNPC) and loss of load probability (LLP) criteria was completed in [25]. The WCA algorithm performed better than the others did. The robust light field semantic segmentation network incorporating contextual and geometric data was introduced by the authors in one work [26]. In another study [27], authors presented an improved adaptive unscented Kalman filter (AUKF)-based power scheduling optimization approach for wind-hydrogen integrated energy systems. The simultaneous diagnosis approach for power switch and current sensor problems in grid-connected three-level neutral point clamped (NPC) inverters was presented by the authors in [28]. For a parallel inverter system, the authors of [29] introduced a unique droop control mechanism to maximize photovoltaic power output. A comprehensive technical, economic, and environmental framework for assessing the rooftop solar potential of ancient residential structures was described by the authors in [30]. In [31], the metaheuristics WOA,

WCA, grey wolf optimizer (GWO) and Salp Swarm Algorithm (SSA) were used for the optimal sizing of a grid-connected PV-Wind-PHS hybrid system with the aim to minimize the cost of energy (COE). The WOA algorithm gave the best energy cost under a well-defined loss of power supply probability.

In [32], the MOGWO algorithm was used for the optimal sizing of a hybrid storage system consisting of PHS (long-term storage) and a battery (short-term storage) integrated with the PV and wind renewable energy system. This study revealed that the hybrid storage system offered better results in terms of energy cost compared to PHS and battery used alone. The multi-objective particle swarm optimization (MOPSO) algorithm was used in [33] for the optimal sizing of a PV-Wind-PHS hybrid system with the objective of minimizing the levelized cost of energy (LCOE) and LPSP. The optimal size of a PV-Wind-PHS hybrid system was carried out on HOMER in [34] using the life cycle cost criteria and the loss of load probability (LOLP), and the authors did not handle the constraints. To solve multi objective functions (two or three objective functions) such as financial and reliability parameters, financial and carbon emissions parameters, reliability and carbon emissions parameters, and financial reliability and carbon emissions parameters, they can be simultaneously evaluated easily by using NSWOA and NSGA-II, since those metaheuristic optimization techniques are more popular, simple to execute, more stable, and faster to converge. The multi-objective NSGA-II [35,36] model has been previously used, which includes two or three objective functions that must be minimized or maximized. NSGA-II successfully converges to a Pareto front, and its programming calculates the best hybrid renewable energy cost of electricity and efficiency for each wind power generation [37,38]. It is possible to use a multi-criteria decision-making technique. The best variables for hybrid renewable energy modeling are successfully obtained from the optimal cost and efficiency solutions [39]. In this paper, NSGA-II is used as a comparison for the main methods, i.e., NSWOA. Because NSWOA had not previously been applied to the optimal size of renewable energy sources in the situation of multiple objective functions, we adopted this metaheuristic optimization technique for solving multiple objective functions of renewable energy generation.

In Cameroon, electrical energy comes mainly from hydroelectric plants. However, thermal power plants continue to be used for electricity generation despite their economic and environmental disadvantages. The migration from these polluting energy sources to renewable energy sources is crucial and therefore deserves to be addressed. The country has a huge potential in renewable energy resources. Indeed, the average sunshine is 4.9 kWh/m^2/day in the southern part of the country and 5.8 kWh/m^2/day in the northern part [40]. The concentration of solar irradiation in the northern part of the country is as shown in Figure 1 and can be found in [41].

Moreover, the international agency of renewable energies evaluates the wind energy potential to be nearly 979 TWh/year [42]. These two sources, if properly exploited, could constitute credible alternatives to the thermal power plants connected to Cameroon's electrical grid. This work focuses on the replacement of thermal power plants in northern Cameroon by PV and wind systems. To have a reliable system, a PHS energy storage system is also dimensioned and connected to the electrical grid. The choice of this type of storage is explained by the presence of a site with the required topographical characteristics close to Lake Lagdo and the electrical grid in northern Cameroon.

Two optimization algorithms, NSWOA and NSGA-II, were used to solve the bi-objective optimization problem whose objective is the minimization of both the total cost of the different components of the renewable energy sources (RES) and the LOLP. These two algorithms have already proved their worth in solving complex optimization problems [43–46]. The results obtained from the two algorithms were compared in order to select the best one. Different study analyses have been developed and evaluated to obtain the best possible scenario between the PV-PHS system, Wind-PHS system and PV-Wind-PHS system for the replacement of thermal power plants.
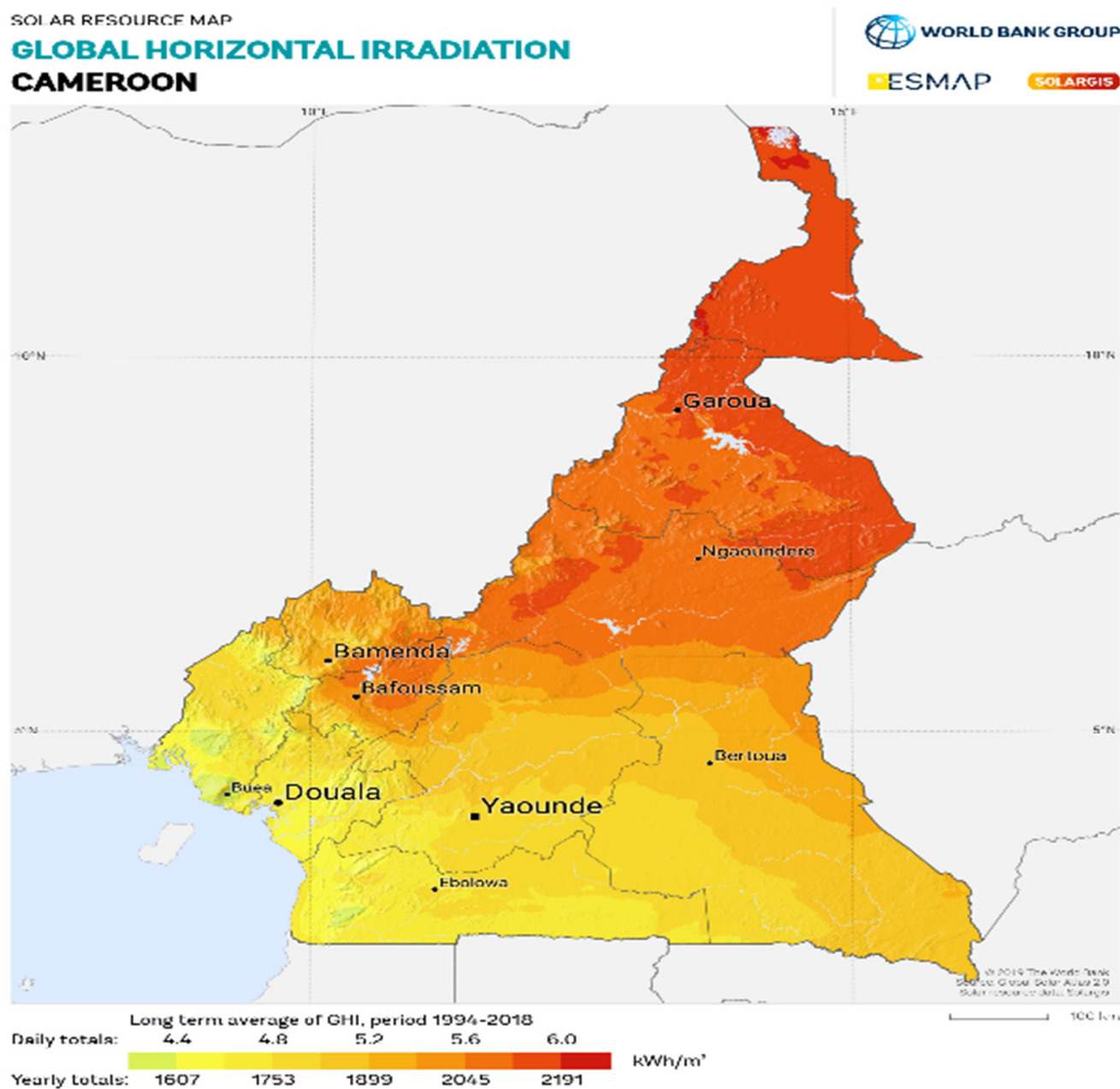
Figure 1. Global horizontal irradiation (1994–2018), Cameroon. © 2020 The World Bank, Source: Global Solar Atlas 2.0, Solar resource data: Solargis.

After thoughtfully examining the research works stated above, it was found that the following issues were not addressed by the current approaches and are therefore addressed in this paper:

- The PV-wind-PHS system is optimally estimated within the limit of the assigned choice of the arbitrary size of the individual system under the upper and lower limit inequality constraints, with a minimum system total cost and zero loss of load probability within the limit of the transmission system capacity.
- The total renewable energy resource power plant carrying capacity limits are determined to achieve the lowest total system cost in various scenarios.
- The adopted NSWOA technique, which was used for the optimal sizing of PV-wind-PHS systems and compared to NSGA-II, has shortcomings that can be addressed in different configurations.

The purpose of this study was to investigate replacing diesel thermal power plants connected to northern Cameroon's interconnected electrical network with a PV-wind-PHS renewable plant in order to reduce the country's reliance on fossil fuels, contribute to environmental preservation, and minimize the country's huge fuel costs. Metaheuristic optimization approaches such as NSWOA and NSGA-II were used to optimally size the proposed system while minimizing the TC and LOLP objective functions.

The main contribution of this work is stated as follows:

- A multi-objective optimization function was carried out to analyze both the profitability and the reliability of a grid-connected RES system for replacing thermal power plants.
- To develop a numerical model that describes the parallel operation of an interconnected energy framework made up of solar PV, WT, and a pumped-storage system that is integrated with the electric utility.
- Proposing a practical method based on the MATLAB software and utilizing the NSWOA and NSGA-II algorithms to efficiently and intelligently reduce the system's size to replacing thermal power plant.
- Investigating and evaluating different configurations, such as a solar PV/WT/PHSS energy storage system, solar PV/PHSS energy storage system and WT/PHSS energy storage system, in an interconnected mode of operation.
- Implementing a detailed comparative analysis, combined with a sensitivity assessment of the economic and reliability indicators for the different HRES configurations.
- Underlining the potential and need for an integrated renewable energy approach in the southern Cameroon transmission network, as well as the economic feasibility and environmental advantages of the proposed solar PV/WT/PHSS energy storage system.

The following is how the remaining portions of the paper are organized: Section 2 introduces the study area, which is followed by a discussion of resource assessment in Section 3, a proposed schematic diagram and mathematical modeling of each RES to obtain accurate and realistic expressions of the solar PV, wind, and pumped hydro storage systems is discussed in Section 4, proposed system operation strategies are discussed in Section 5, evaluation of design parameters occurs in Section 6, formulation of the optimization problem are expressed in Section 7, results and discussion are in Section 8, and conclusions and discussion are expressed in Section 9.

2. Presentation of the Study Area

The interconnected grid in northern Cameroon provides electrical power to the population of three regions representing the entire northern part of the country. The main source of energy production on this network is the Lagdo hydroelectric dam built between 1977 and 1982 [47]. Due to the rapid growth of the population in this part of Cameroon as well as climate warming, this hydroelectric power station is no longer able to meet all of the demand on the electrical network. Climate change is anticipated to diminish hydro-energy generation by 20% during the worst seasons [48]. Thus, for a total basic capacity of 72 MW, the power plant nowadays only operates at about 40 MW. In 2019, the annual energy production of the Lagdo hydroelectric dam represented approximately 5% of the total energy consumed in Cameroon, or about 350.315 GWh [49]. Diesel thermal power plants have been installed to compensate for the reduced power supplied by the Lagdo hydroelectric dam in Garoua and Maroua. The Djamboutou thermal power plant on the outskirts of Garoua has a total capacity of 20 MW and the one in Maroua has a total capacity of 10 MW. The peak power generation on the grid is about 62 MW and the minimum power generation is 47 MW as shown in Figure 2.
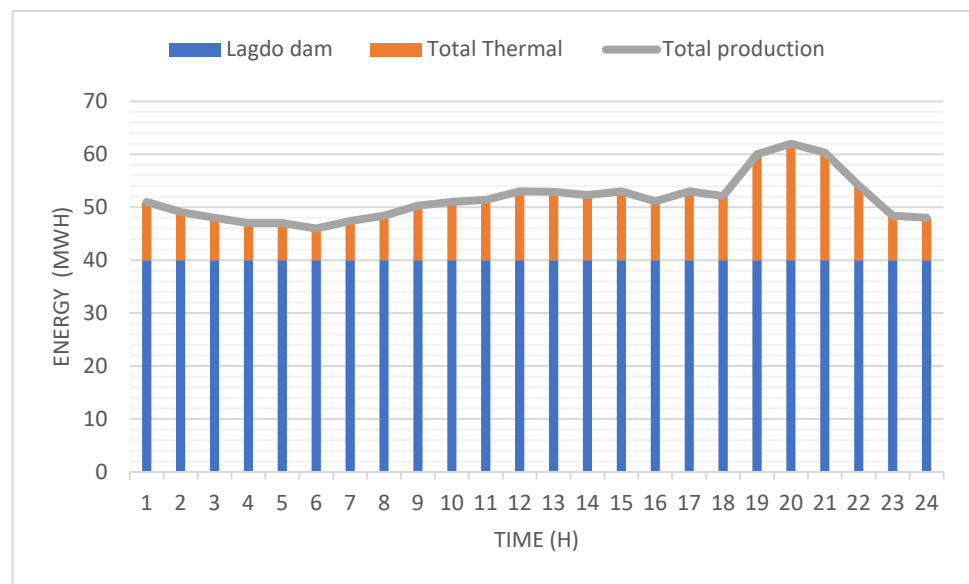
Figure 2. Total energy production on Northern Interconnected Grid, Cameroon.

3. Resource Assessment

3.1. Solar Resource

The Cameroonian territory benefits from a rather important sunshine potential, especially in the northern part as shown in the Figure 1. The average annual radiation variation varies from 4–4.9 kWh/m^2/day in the southern part to 5.8 kWh/m^2/day in the northern part of the country [40]. Concerning the northern part of the country, which is the subject of this study, the solar potential appears to be enormous. Figure 3, which presents the irradiation and average monthly temperature data for the period of one year obtained from [50], allows us to measure the solar potential in the Garoua area (Latitude 9°18′25.2″ N and Longitude 13°23′34.8″ E) where the Djamboutou thermal power plants are located. The city of Garoua is one of the major cities of northern Cameroon, with Maroua located further north. All this justifies the choice of this zone for the installation of a PV system connected on the northern integrated grid (NIG) since it is close to the installation site of the PHS system and to a big city.
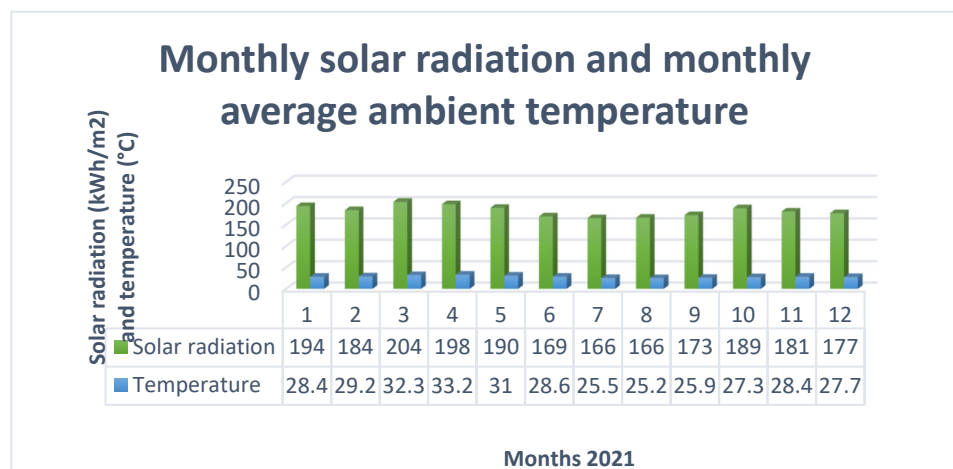

Figure 3. Monthly solar radiation and average ambient temperature.

3.2. Wind Resource

The wind energy potential in the far north of Cameroon is not negligible, especially for large-scale applications. The city of Maroua, the second largest in the north, has the

meteorological assets necessary for the installation of wind power plants as revealed in [51]. Being one of the major urban centers of the region, the town of Maroua is an optimal location for the installation of a power plant because of its proximity to consumers. Figure 4 shows the monthly average wind speed at Maroua outskirts (Latitude 10°37′48″ N and Longitude 14°21′7.2″ E) at a height of 10 m [52].
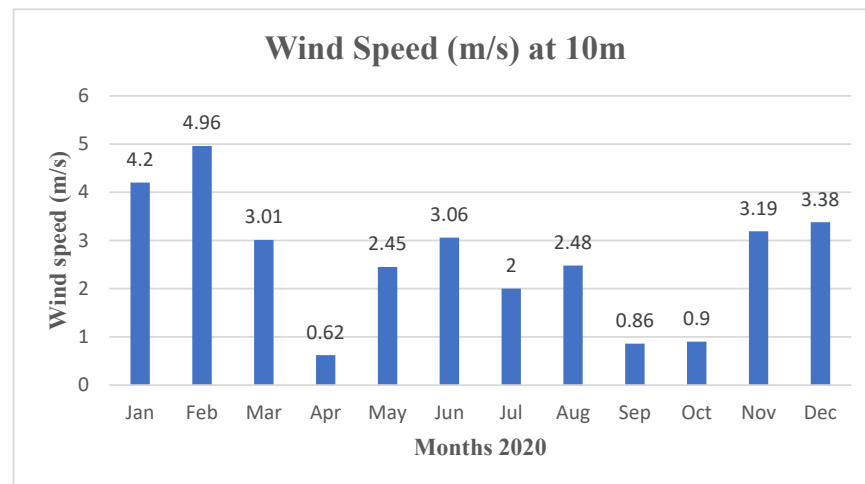
Figure 4. Monthly average wind velocity at 10 m height.

3.3. PHS Potential

The potential for large-scale installations of PHS systems is primarily dependent on the availability of water resources and space at a high enough altitude to have sufficient potential energy. According to a study [53], there is an exploitable region of roughly 6.8 hectares positioned at 260 m from the lake level that has the required features for the installation of a PHS system with a maximum capacity of 841 MWh around Lake Lagdo and near Garoua. Combining the maps depicting the global irradiation of the entire country of Cameroon [41] and the location of the PHS system using Google Maps [54] yields Figure 5.

Figure 5. Favorable location for installation of PHSS near Lagdo Lake.

4. Proposed Schematic Diagram

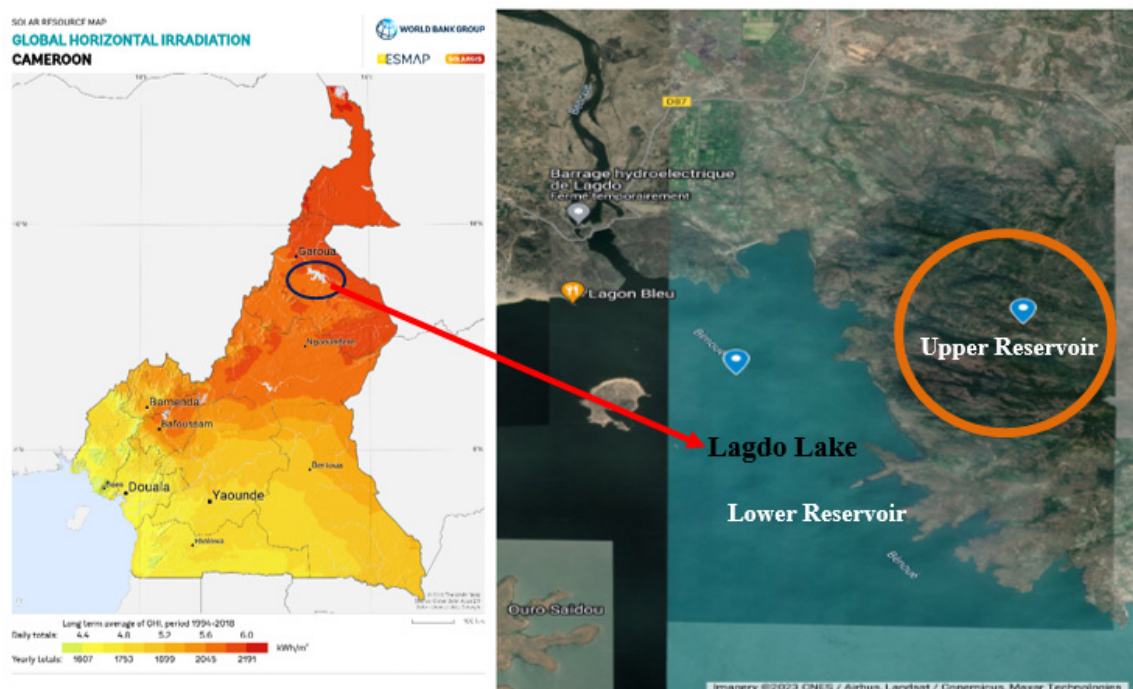The proposed system to replace the LFO thermal power plants in northern Cameroon consists of a solar photovoltaic power plant in the vicinity of Garoua and a wind power plant in the commune of Maroua. As both of these renewable energy sources are intermittent, an energy storage system here the PHS system will be coupled to the power grid to make it more reliable and resilient. Figure 6 describes the suggested schematic diagram of the renewable energy resource configuration.
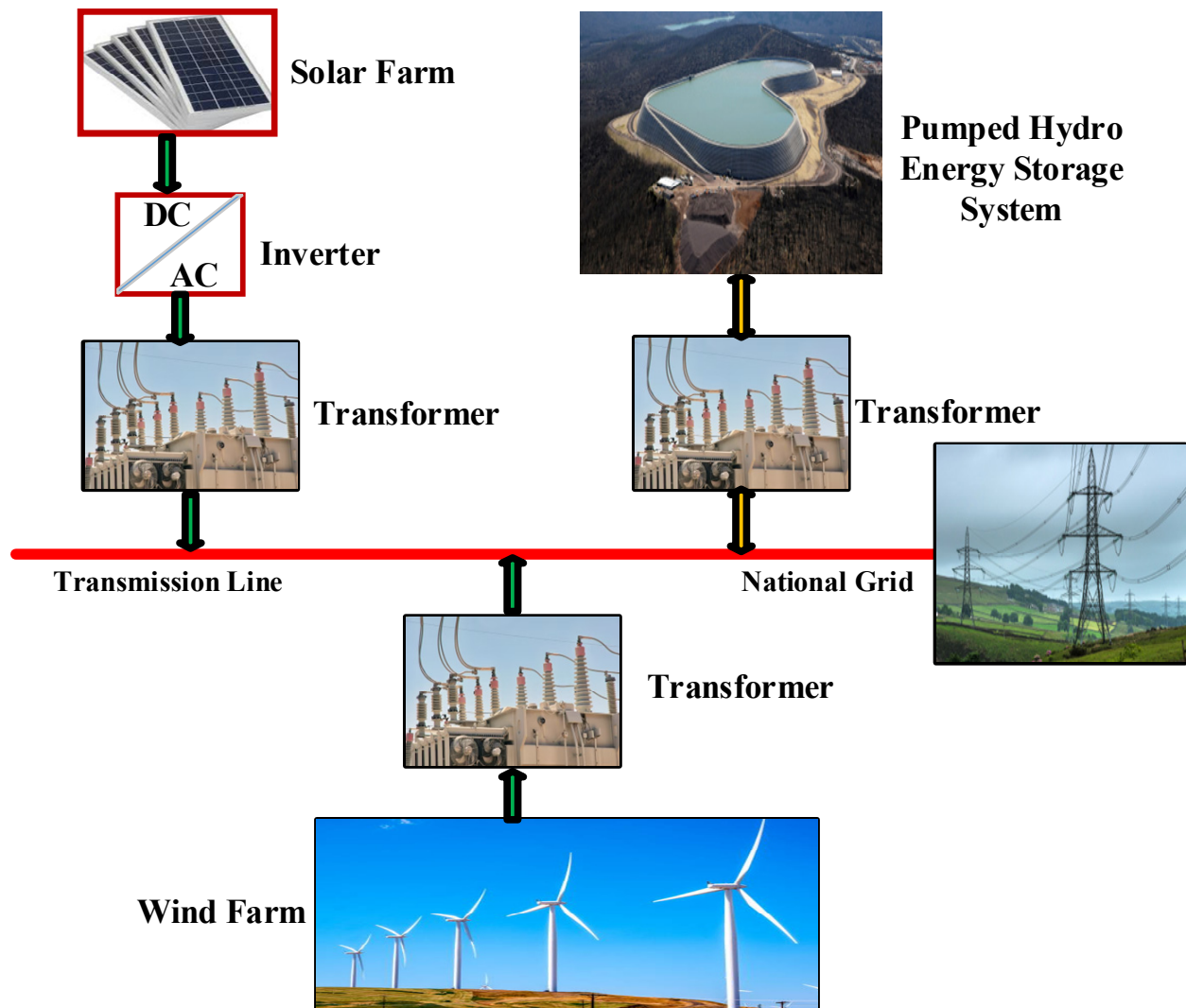
Figure 6. Schematic diagram of the grid-connected solar PV/Wind/PHES system.

4.1. Mathematical Modeling of RES

The knowledge of the mathematical and economic models of all the renewable energy production sources and the two storage systems are essential for the optimal dimensioning of each component.

4.1.1. Solar Photovoltaic Generation System

Solar cells convert sunlight into electrical energy. As shown in Equation (1) below, the power generation of a solar panel is dependent on its surface A, the amount of radiation it receives $G(t)$, and its efficiency η_{pv}, which has been used in multiple works [23,55,56]. As input, the model utilizes hourly solar radiation and temperature data. It is given by:

$$P_{PV}(t) = A \times G(t) \times \eta_{pv} \tag{1}$$

The efficiency η_{pv} of solar panels is determined by reference efficiency η_r, temperature constant β, performance degradation factor η_{pc}, ambient temperature T_a, and solar radiation. It is given by [23,55,56]:

$$\eta_{pv} = \eta_r \times \eta_{pc} \times \left[1 - \beta \left(T_a + \left(\frac{NOCT - 20}{800} \right) \times G(t) - T_{cref} \right) \right] \tag{2}$$

4.1.2. Inverter

The inverters in this study are directly coupled to the solar panel pack. They are therefore unidirectional inverters in charge of converting the energy in DC form into AC energy. Equation (3) translates the necessary constraint on the total inverter capacity to be installed as a function of the total power installed for the PV system. The characteristics of the inverters used in this study are presented in Table 1.

$$P_{inv} \geq P_{peak-PV} \tag{3}$$

4.1.3. Wind Power Generation System

The power produced by wind turbines depends on the kinetic energy of the wind. The expression for the output of the wind field is described by Equation (4) [46,57,58]:

$$P_{WT}(v) \begin{cases} 0 & , \ v < v_{ci} \\ P_{rated} \times \frac{v - v_{ci}}{v_r - v_{ci}} & , \ v_{ci} \leq v \leq v_r \\ P_{rated} & , \ v_r \leq v \leq v_{co} \\ 0 & , \ v > v_{co} \end{cases} \tag{4}$$

From the Equation (4), the output power of WT is zero below v_{ci} and above v_{co}, and the output power increases linearly with increasing wind speed between v_{ci}, and v_r and it generates the rated power between v_r and v_{co}.

Equation (5) [20,59], allows us to calculate the wind speed v at any hub height z from the wind speed v_0 at a given height z_0 and α.

$$v(z) = v_0 \times \left(\frac{z}{z_0} \right)^{\alpha} \tag{5}$$

where v is the wind speed at height z, v_0 the wind speed at the reference height z_0, and α the Hellman exponent that is often considered equal to 1/7, but which will be calculated by Equation (6) [33] in this study.

$$\alpha = \frac{0.37 - 0.088 \ln(v_0)}{1 - 0.088 \ln(z_0/10)} \tag{6}$$

4.1.4. Pumped Hydro Storage System

In this work, the PHS system operates in a very traditional manner. The flow of energy in the electrical network is constantly monitored. When there is excess energy in the electrical grid and the PHS system's upper water reservoir is not full, the PHS system goes into pumping mode for as long as there is excess energy and the upper reservoir is not full. When the two sources (photovoltaic and wind fields) are unable to meet all of the demand previously met by the thermal plants, the PHS system switches to power generation mode to supply the resulting energy deficit. The Lagdo hydroelectric dam serves as the North Cameroon power system's base load.

a. Energy Balance: The energy balance here is the difference between the energy production from the solar P_{PV} and wind P_{WT} fields and the energy demand met by the LFO thermal plants P_{DT}.

$$E_B(t) = N_{PV} \times P_{PV}(t) \times \eta_{inv} + N_{WT} \times P_{WT}(t) - P_{DT}(t) \tag{7}$$

b. PHSS Generating Mode: If $E_B(t) < 0$, the demand is greater than the PV and wind systems' output. In this case, the energy must be supplied by the PHS system. The power delivered by the PHS depends on the amount of water available in the upper reservoir, power rating of the PHS system, and the energy demanded. If there is enough water in the upper reservoir, the energy requirements of the loads will be met. Otherwise, the PHS system will do its best. The Equations (8) and (9) are inspired by the models utilized in the papers [23,31], and translate the operation of the PHS in generating mode.

$$E_{PHS}(t) = min\left\{ \left(\frac{V(t-1) - V_{min}}{3600} \right) \times g \times \rho \times \eta_t \times H, min(P_{PHSn}, |E_B(t)|) \right\} \tag{8}$$

$$q_{dis}(t) = \frac{E_{PHS}(t)}{g \times \rho \times \eta_t \times H} \tag{9}$$

Here, the density of water ρ and the gravitational constant g are assumed to be 1000 m^3/kg and 9.81, respectively. H is the sum of the height of the water level in the upper reservoir and the elevation of the upper reservoir location above Lagdo Lake. It is calculated by Equation (10).

$$hadd(t) = \frac{V(t-1)}{area} \tag{10}$$

$$H(t) = h + hadd(t) \tag{11}$$

The height induced by the water level in the upper tank depends on the type of structure adopted for its construction. Equation (10) allows us to evaluate it for a specific type of construction structure. Considering the height h of the selected site in relation to the Lagdo Lake, which is 260 m, this additional height is neglected in this work.

The Equation (12) determines the power P_{PHS} supplied by the PHS system to the loads [60].

$$P_{PHS}(t) = q_{dis} \times g \times \rho \times \eta_t \times H \tag{12}$$

c. PHSS Pumping Mode: If $E_B(t) > 0$, there is excess energy in the power grid. If the upper reservoir is not full, the PHS switches to pumping mode until the upper reservoir is filled. The amount of water pumped is determined by the reservoir's water level, the amount of excess power available from the grid, and the power rating of the PHS system.

$$E_P(t) = min\left\{ \left(\frac{V_{max} - V(t-1)}{3600} \right) \times g \times \rho \times H \times \frac{1}{\eta_P}, min(P_{PHSn}, E_B(t)) \right\} \tag{13}$$

$$q_{ch}(t) = \frac{\eta_P \times E_P(t)}{g \times \rho \times H} \tag{14}$$

In pumping mode, the power consumed over time by the PHS system is calculated using Equation (15) [60].

$$P_P(t) = \frac{\rho \times g \times q_{ch}(t) \times H}{\eta_P} \tag{15}$$

d. Surplus Energy: Excess energy in the electrical grid only occurs when the PHS system is operating in pumping mode ($E_B(t) > 0$). When the energy produced by the RES is greater than the demand, if the upper reservoir is not completely filled, the

PHS system goes into pumping mode. If the available energy is greater than the consumption of the PHS system in pumping mode, then the difference between the available energy and the consumption of the PHS system represents surplus energy. If the upper reservoir is filled, then the PHS stops operating in pumping mode, and all available energy becomes surplus energy on the grid. The Equation (16) expresses the surplus energy on the power grid.

$$E_S(t) = E_B(t) - E_P(t) \tag{16}$$

e. Model of the Reservoirs: The volume $V(t)$ of water in the upper reservoir at time t is a function of the volume of water pumped $q_{\text{ch}}(t)$, the volume of water used to generate electricity $q_{dis}(t)$, the volume $V(\text{t}-1)$ of water present in the reservoir at time t − 1, and the rate of evaporation and leakage over time γ. The following expression determines the amount of water available in the upper reservoir:

$$V(t) = (1 - \gamma) \times V(\text{t}-1) + \Delta\text{t} \times (q_{\text{ch}}(t) - q_{dis}(t)) \tag{17}$$

The volume of water in the upper reservoir varies between the minimum and maximum water volumes set for the reservoir: $V_{min} \leq V(t) \leq V_{max}$.

The total amount of energy stored in the upper reservoir E_C in kWh is calculated by the Equation (18) [61]:

$$E_C = \frac{\eta_t \times g \times \rho \times V_{max} \times H}{3.6 \times 10^6} \tag{18}$$

4.1.5. Utility Grid

The power transiting through the NIG transmission network is obtained by Equation (19).

$$P_{grid}(t) = P_{LD}(t) + N_{WT} \times P_{WT}(t) + N_{PV} \times P_{PV} \times \eta_{inv} + P_{PHS}(t) \tag{19}$$

where P_{LD} represents the power produced by the Lagdo dam, which is constant and represents the base load of this grid. The power flowing through the network is subject to the constraint expressed by Equation (20).

$$0 \leq P_{grid}(t) \leq P_{grid}^{max} \tag{20}$$

P_{grid}^{max} represents the maximum power that can be transmitted on the electrical grid.

4.2. Technical and Economical Specification of Components

The technical and economic parameters of the components used in this work are summarized in Table 1. The costs of the PV and wind systems are the costs published by the International Renewable Energy Agency (IRENA) in 2022 for the year 2021 [62]. The costs associated to the construction of the PHS system are obtained from [63].

Table 1. Technical and economic parameters of the components.

Solar Panel	
Model	LUM 24380 MP
Power peak	380 Wp
A	1.976 m × 0.991 m
NOCT	45 °C
η_r	19.41%
β	0.41%

Table 1. *Cont.*

Solar Panel	
C_{i-PV}	857 €/kW
$C_{O\&M-PV}$	1%
Life span	25 years
Wind Turbine	
Model	GW 150–3.0 MW (PMDD Smart Wind Turbine) [64]
P_{rated}	3 MW
$v_{ci}/v_r/v_{co}$	2.5/9/18 m/s
Rotor diameter	150 m
Height	95/120/140 m
C_{i-WT}	1325 €/kW
$C_{O\&M-WT}$	3% of capital cost
Life span	+20 years
Inverter	
Model	SMA Sunny High-power Peak3 SHP 150-20
DC Power	150 kW
Efficiency	98%
C_{i-Inv}	7548 €
$C_{O\&M-Inv}$	1%
Life span	Above 20 years [65]
PHS system [20]	
$\eta_t \times \eta_p$	75%
C_{i-PHS}	513 €/kW
Cost of balance	15 €/kW
C_S	68 €/kWh
$C_{O\&M-FPHS}$	4.6 €/kW
$C_{O\&M-VPHS}$	0.22 €/MWh
Economic parameters	
d	7%
f	3%
Lifetime of the project	20 years
Algorithm parameters	
Iteration	200
Population number	200

5. Proposed System Operation Strategies

The careful monitoring of the energy flow in the power grid is necessary for the projected renewable energy system to replace thermal power plants. Equation (7) provides an evaluation of the disparity between the amount of energy generated by wind and solar power plants and the demand. The PHS system enters water-pumping mode to fill the upper reservoir if the RES generation is more than the overall energy demand and the upper reservoir is not full. This process continues as long as the upper reservoir is not full and the RES output is greater than the demand. The quantity of energy used by the PHS system and the pace at which water is pumped are shown in Equations (13) and (14) respectively. The energy surplus is determined by the difference between the extra energy and the energy used. The PHS system, on the other hand, is activated in energy-generating mode and is responsible for delivering the missing energy in accordance with the quantity of water present in the upper reservoir when the demand is greater than the energy generated by the RES. The quantity of energy generated by the PHS system and the water flow rate necessary to create this energy are translated by Equations (8) and (9) respectively. As long as the top reservoir has more water than the specified minimum threshold, the PHS system generates energy to meet the energy requirement. Finally, if the RES and PHS systems fail to meet all the demand, the criterion measuring the reliability of the system evaluates, in this study, the probability in terms of time of the energy deficit. In this case, the overall operation and energy flow can be performed as shown on the flowchart in Figure 7.
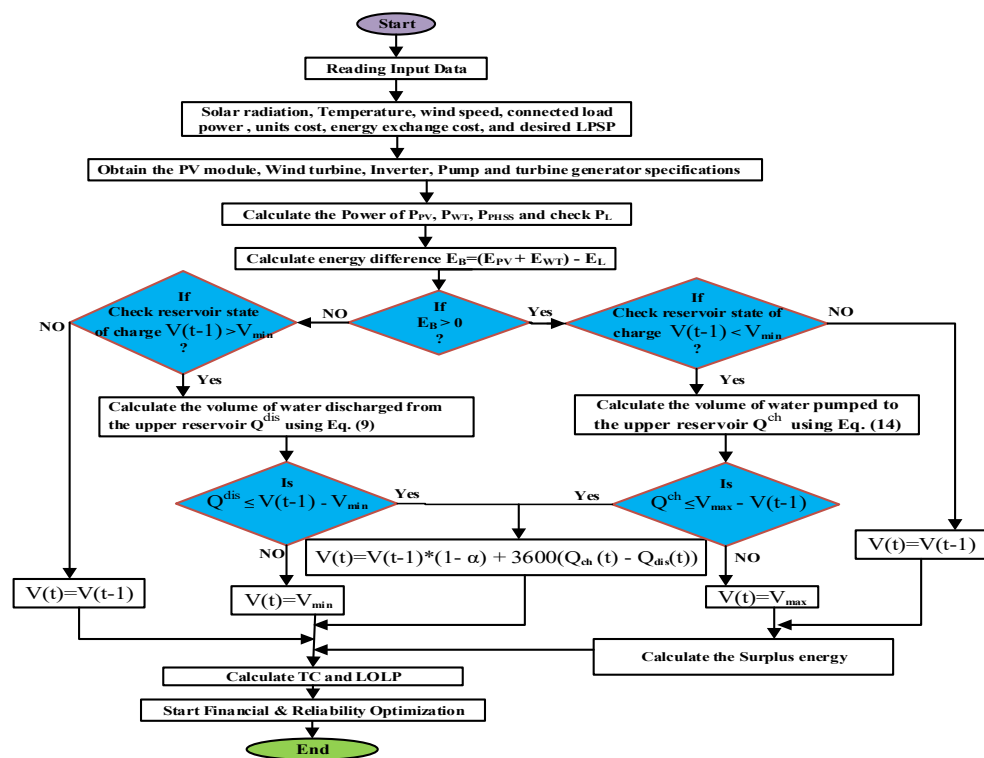
Figure 7. A Flowchart describing an operation of a proposed grid-connected solar PV/Wind/ PHES system.

6. Evaluation Parameters

6.1. Reliability of the System

To measure the reliability of the new grid configuration by the substitution of LFO thermal power plants by PV and Wind systems, the criterion measuring the hourly energy deficit rate was implemented in this study. This criterion is the loss of load probability (LOLP).

LOLP

LOLP in this study is the probability that the electricity demand currently met by LFO thermal plants will exceed the generation capacity of PV and wind plants over a period of time. An LOLP analysis is done hourly over a one-year period. The LOLP is used to measure the reliability of the new generation system configuration in relation to the electricity demand. This is the main criterion that determines the size of the green energy systems to be installed. Its expression is transcribed by the Equation (21) [19] and Equation (22).

$$LOLP = y\{f(x) \leq 0\} = \frac{1}{N}\sum_{1}^{t} F_y \tag{21}$$

$$f(x) = N_{PV} \times P_{PV}(t) + N_{WT} \times P_{WT}(t) + P_{PHS}(t) - P_{DT}(t) \tag{22}$$

In this instance, N = 8760 is the simulation period, and F is the failure frequency of the response y when it is negative.

6.2. Economic Model

Several economic criteria were considered in this work. These are the TC of the project over its lifetime, the LCOE evaluated for each energy production system and the NPV for each scenario studied.

6.2.1. Total Cost

The total cost takes into account the initial capital cost, the operation and maintenance cost, the replacement cost of components and the salvage cost at the end of the project life [66,67].

$$TC = C_{initial} + C_{replace} + C_{O\&M} - C_{savage} \tag{23}$$

The salvage cost has been neglected in this study.

The total cost over the study period of each source of renewable energy generation and energy storage was evaluated.

a. PV System: The total cost of the PV system considers the total cost of the PV system and the PV inverters. It includes the initial cost and the cost of operations and maintenance. Considering the duration of the project (20 years) considered in this study, no component replacement will be made. It is calculated by Equation (24):

$$TC_{PV} = N_{PV} \times C_{i-PV} + N_{PV} \times C_{O\&M-PV} \times k + N_{Inv} \times C_{i-Inv} + N_{Inv} \times C_{O\&M-Inv} \times k \tag{24}$$

The life-value discount factor k depends on the rate of inflation f and the nominal interest rate d. It is provided by Equation (25) [68,69].

$$k = \frac{(1+ir)^n - 1}{ir(1+ir)^n} \tag{25}$$

$$ir = \frac{d-f}{1+f} \tag{26}$$

b. Wind System: The total cost over the lifetime of the wind power plant includes the initial installation cost and the cost of maintenance and operations. It is determined by Equation (27).

$$TC_{WT} = N_{WT} \times C_{i-WT} + N_{WT} \times C_{O\&M-WT} \times k \tag{27}$$

c. Storage System: The total cost of the PHS system includes not only its initial investment, but also its fixed and variable operating and maintenance expenses. It is computed using the Equation (28).

$$TC_{PHS} = P_{PHSn} \times C_{i-PHS} + E_c \times C_S + (P_{PHSn} \times C_{O\&M-FPHS} + E_{PHS} \times C_{O\&M-VPHS}) \times k \tag{28}$$

C_{i-PHS} is expressed in €/kW, C_S in €/kWh, $C_{O\&M-FPHS}$ in €/kW, and $C_{O\&M-VPHS}$ in €/MWh.

6.2.2. LCOE

The levelized cost of energy is used to calculate the lifetime cost of producing energy from a power plant. It is determined by [70,71]:

$$LCOE = \frac{TLCC}{\sum_{i=1}^{n} \left(\frac{E_t}{(1+ir)^n} \right)} \tag{29}$$

where E_t is the annual energy produced in each source. The TLCC represents the total life-cycle cost of the project, which includes capital, operating, and maintenance costs over the life of the project. This cost amounts to the total cost of the project over its lifetime. The LCOE will be evaluated for each energy generation source.

6.2.3. NPV

The criteria for measuring a project's cash flow were implemented to evaluate the profitability and payback time of the proposed new systems. The following equation expresses the NPV [72]:

$$NPV = \sum_{i=1}^{n} \frac{C_t}{(1+ir)^i} \qquad (30)$$

7. Formulation of the Optimization Problem

This study's bi-objective optimization issue considers both the dependability and the cost of the development of renewable energy facilities. The overall cost function, which depicts the total cost of the PV, wind, and PHSS plants, and the LOLP function, which gauges the ability of renewable energy sources to meet demand, are the two objective functions that have been implemented. Equation (31) presents the expression translating the optimization issue. The quantity of solar panels, wind turbines, the maximum installed power of PHSS, and the sizes of the upper reservoir are the optimization factors used for this issue. There are limitations imposed on the optimization issue by Equation (32). Several scenarios have also been studied to solve this optimization problem. These are the scenarios where only the solar system and PHS are considered or the wind system and PHS are considered. This allows for a comparative analysis of the results in order to choose the best configuration.

$$min\begin{cases} \sum TC_i \\ LOLP \end{cases} = min\begin{cases} TC_{PV} + TC_{Wind} + TC_{PHS} \\ LOLP \end{cases} \qquad (31)$$

$$\begin{cases} N_{PV}^{min} \leq N_{PV} \leq N_{PV}^{max} \\ N_{Wind}^{min} \leq N_{Wind} \leq N_{Wind}^{max} \\ P_{PHSn}^{min} \leq P_{PHSn} \leq P_{PHSn}^{max} \\ V_{nmin} \leq V_{max} \leq V_{nmax} \\ V_{nmin} \leq V_{max} \leq V_{nmax} \\ P_{inv} \geq P_{peak-PV} \end{cases} \qquad (32)$$

7.1. Optimization Algorithm

7.1.1. Non-Dominated Sorting Whale Optimization Algorithm (NSWOA)

The non-dominated sorting optimization technique has been combined with the whale optimization algorithm (WOA) to develop a hybrid algorithm inspired by nature [45]. Solving multi-objective optimization issues with often conflicting objective functions, where minimizing one leads to maximization of the other, necessitates an optimal trade-off between the objective functions. The non-dominated sorting technique begins by sorting a set of Pareto-optimal solutions that can be termed ideal. The Pareto-optimal value is obtained from the Pareto-optimal solutions to distinguish between dominated and non-dominated datasets [73]. Sorting, as previously stated, is accomplished by bringing the best answers to the head of the queue through non-dominated sorting of their rank values. The generated non-dominated sorted solutions are then optimized using the WOA technique to get a better and more efficient outcome in less time. The whale optimization algorithm is divided into three phases. Humpback whales circle their target in the first stage, and then assault their prey using bubble-hunting methods in the second stage. Finally, the whales resume their search for prey in a random manner based on the position of other whales [74]. NSWOA's step-by-step method is as follows [45,74]:

Step 1: Initializing the system parameters, determining the number of iterations, and generating the initial population constitute the initial step.

Step 2: The relevance function is used in this step to assess the relevance of each search agent.

Step 3: The initially generated search agents are sorted based on their fitness value in this step. To sort the search agents, the non-dominated sorting technique is employed. The crowding distance and current population ranking are then computed.

Step 4: The positions of the search agents are iteratively updated to increase the pressure on the target. When in search of food, humpback whales, which represent the search agents, will select the optimal solution as their primary quarry. The following equations describe the whales' encircling behavior if $\vec{X}^*$ is considered the optimal location at the present time.

$$\vec{D} = \left| \vec{C}.\vec{X}^*(t) - \vec{X}(t) \right| \tag{33}$$

$$\vec{X}(t+1) = \vec{X}^*(t) - \vec{A}.\vec{D} \tag{34}$$

where $\vec{X}$ represents the position vector, and t represents the number of iteration; $\vec{A}, \vec{D}$ represent co-efficient vectors, which are updated to adjust the latest position of the prey around the search agent, as shown in the following equations:

$$\vec{A} = 2\vec{a}.\vec{r} - \vec{a} \tag{35}$$

$$\vec{C} = 2\vec{r} \tag{36}$$

Here, $\vec{a}$ decreases linearly from 2 to 0 as the iteration progresses, which makes $\vec{A}$ vary in $[-a, a]$ range, and $\vec{r}$ is a random vector between [0, 1].

Step 5: Spiral positioning update of humpback whales is performed to replicate their helix-like motion. The search agent positions are updated using Equation (37).

$$\vec{X}(t+1) = \vec{D}'.e^{bl}.\cos(2\pi l) + \vec{X}^*(t) \tag{37}$$

where b defines the shape of the logarithmic spiral motion of the whales and is a constant value, l is a random number between $[-1, 1]$, and $\vec{D}' = |\vec{X}^*(t) - \vec{X}(t)|$ indicates the distance between the prey position $\vec{X}'$ and the search agent position $\vec{X}$.

Step 6: The position of the whales can be updated in one of two ways: by decreasing or reducing the circling procedure, or by employing the spiral model. Therefore, the probability is denoted by p, a random number between 0 and 1. In this step, an if–then condition is executed to accomplish the goal. If random number p is less than 0.5 and A is less than 1, the search agent's position is updated using Equations (33) and (34). Alternatively, if p is less than 0.5 and A is greater than or equal to 1, a random search agent is selected and its position in the current population is denoted by $\vec{X}_r$. Equation (38) determines the distance between a random search agent and its prey for that agent. In addition, the position of the search agent is updated using Equation (39).

$$\vec{D} = \left| \vec{C}.\vec{X}_r - \vec{X} \right| \tag{38}$$

$$\vec{X}(t+1) = \vec{X}_r - \vec{A}.\vec{D} \tag{39}$$

Step 7: Equation (37) is used to update the search agent's position if the conditions in Step 6 are not met and $p \geq 0.5$.

Step 8: This step evaluates the whale search agent's fitness function values, N_f.

Step 9: The initial generation of fitness function values, O, is merged with the new WOA-optimized fitness values, N_f, to create a solution vector of length $O + N_f$.

Step 10: The new solution vector is non-dominated and sorted. Steps 4 through 10 are looped until the maximum number of iterations is reached.

Step 11: At the conclusion of the loop, the optimal solution is identified as the best available position of the search agent.

7.1.2. Non-Dominated Sorting Genetic Algorithm-II (NSGA-II)

This K. Deb [60], Ref. [62] proposed this NSGA-II algorithm. It includes a selection operator based on a crowding distance computation that estimates the population density for each individual. This algorithm is one of the most popular today because it employs an elitist approach that allows for the preservation of the best solutions discovered in previous generations, it employs a faster sorting procedure based on non-dominance, and it incorporates a different comparison operator based on the calculation of the "crowding" distance. The following describes how the NSGA-II algorithm works: at each cycle, a population of size N is formed from the parent population. The two populations are then blended to generate a 2N population. This gathering ensures elitism. To identify the different fronts, the population of size 2N is then sorted using a non-dominance criterion. The most talented people will be located on the first front or fronts. As long as the population does not exceed N, a new parent population is generated by adding the full fronts. If the number of people present is fewer than N, the crowding technique is used on the next front, which is not part of the new parent population. This operator's purpose is to insert the best people who are absent from the new parent population. This front's individuals are used to compute the crowding distance between two neighboring solutions. After identifying the individuals in the new parent population, the following processes are taken to establish a new child population: selection, crossover, and mutation. The process is repeated from generation to generation until a stopping requirement is met. Here is a detailed technique broken down into numerous phases.

Step 1: Combine the populations of parents Pt and children Qt all of size N and create $Rt = Pt \cup Qt$ and then apply a non-dominated sort on Rt and identify the different fronts: $k = 1, \ldots$, etc.

Step 2: Create a new population $Pt + 1 = \varnothing$ and initialize $k = 1$. As long as $|Pt + 1| + |Fk| < N$ (the population is not full), do $Pt + 1 = Pt + 1 + Fk$ and $k = k + 1$.

Step 3: When all solutions in Fk cannot be included in $Pt + 1$, sort the crowding distances and include in $Pt + 1$ the most scattered $N - |Pt + 1|$ solutions using the crowding distance in the Fk set.

Step 4: Create the child population $Qt+1$ from $Pt + 1$ using distance crowding-based tournament selection and genetic operators (selection, crossover and mutation). Increment the generation counter ($t = t + 1$) until reaching the stopping conditions.

8. Results and Discussion

8.1. Meteorological Data

The meteorological data used can be found at [75]. The wind speed data are an hourly average over five successive years between 2016 and 2020. This allowed having data that are more reliable. With the formula stated in Equation (4), we determined the wind velocity at the height of 140 m. Figures 8 and 9 show the hourly irradiation and temperature, and wind velocity data.

8.2. Presentation of the Results

The results obtained for the three simulation scenarios for each algorithm are presented in Table 2 and Figures 10 and 11. The shape of the curves obtained for the results of the optimization problem is typical of problems where the minimization of one of the functions leads to the increase of the other. Independently of the algorithm and even of the scenarios, the decrease towards zero of the LOLP leads to a rather sharp increase of the total cost and vice versa.
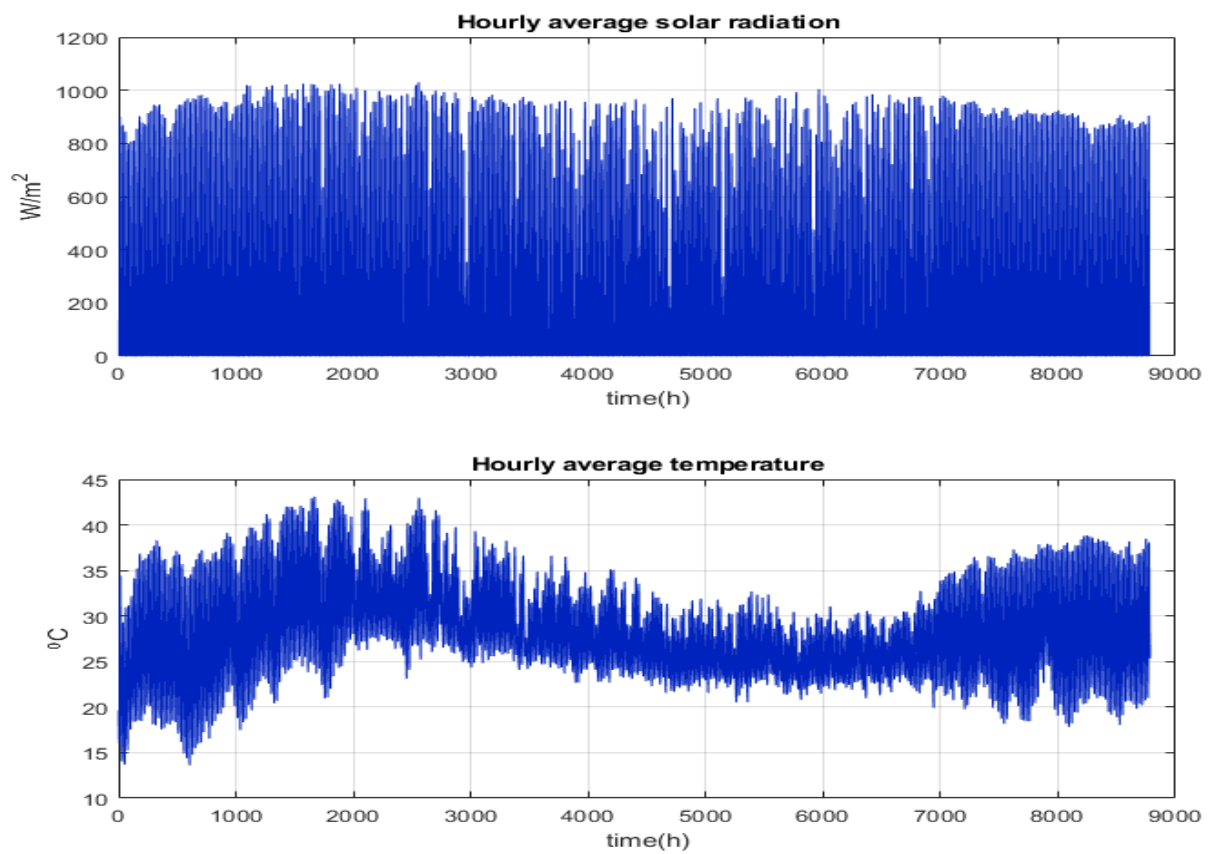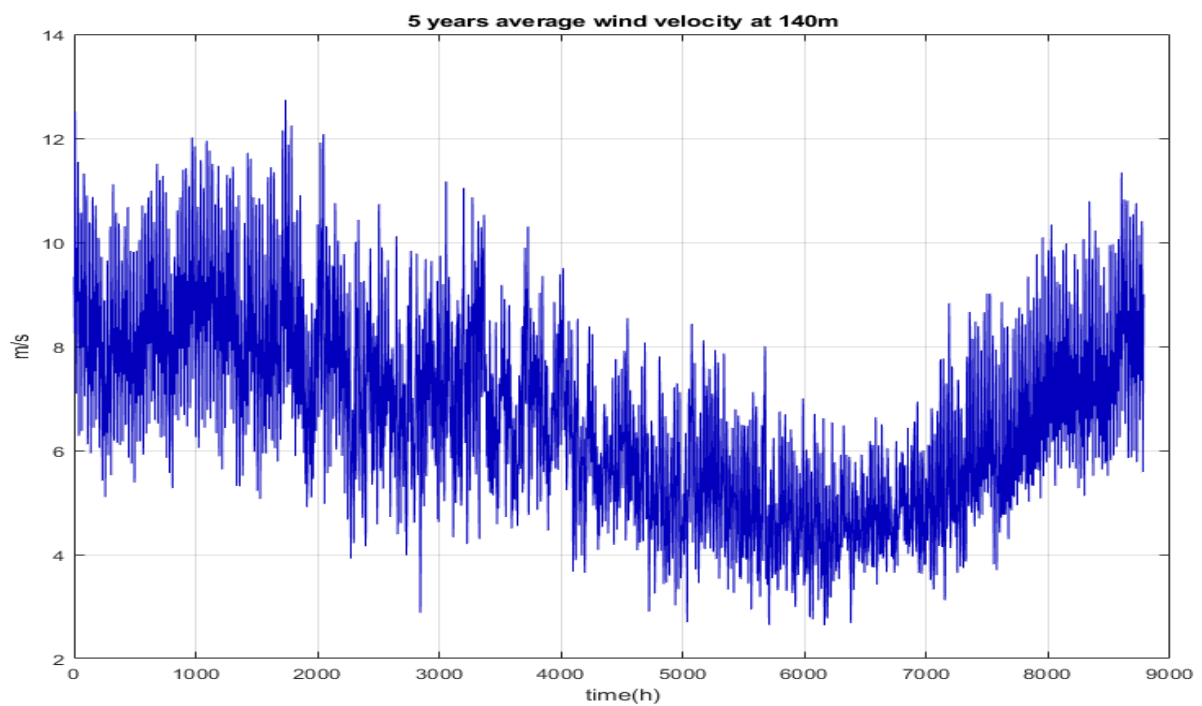
Figure 8. Hourly solar radiation and ambient temperature.

Figure 9. 5 years average hourly wind velocity at 140 m.

Table 2. Results obtained from the simulation.

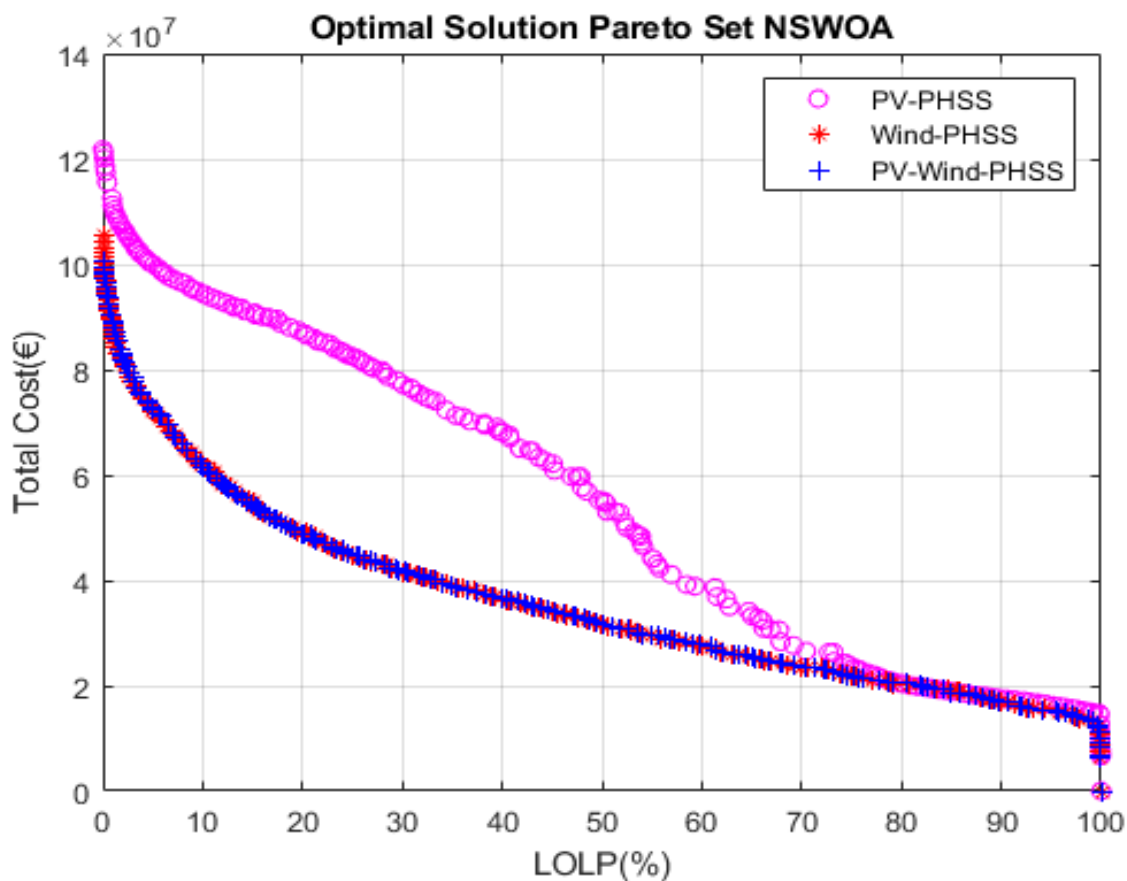|	NSWOA			NSGA-II		
Evaluation Parameters	**PV-PHS**	**Wind-PHS**	**PV-Wind-PHS**	**PV-PHS**	**Wind-PHS**	**PV-Wind-PHS**
LOLP (%)	0	0	0	0	0	0
Total cost (€)	121,760,835	105,596,880	100,749,018	122,814,628	112,470,873	100,969,133
Total cost PV (€)	73,434,451	0	18,471,178	76,595,316	0	25,064,527
Total cost Wind (€)	0	79,136,177	56,124,948	0	89,799,918	50,512,453
Total cost PHS (€)	48,326,383	26,460,702	26,152,890	46,219,312	22,670,955	25,392,151
LCOE_PV (€/kWh)	0.042	0	0.042	0.042	0	0.042
LCOE_Wind (€/kWh)	0	0.025	0.025	0	0.025	0.025
LCOE_PHSS (€/kWh)	0.061	0.385	0.231	0.051	0.424	0.191
PV output power (MW)	71.159	0	17.894	74.225	0	24.289
Wind output power (MW)	0	43	30	0	48	27
PHS power (MW)	35	21.230	22.146	34.907	21.215	22.411
Upper reservoir volume (m^3)	645,956	326,864	306,658	597,696	238,000	284,978
Daily energy storage capacity (MWh)	403.82	204.34	191.71	373.65	148.79	178.15
Number of inverter	475	0	120	495	0	162

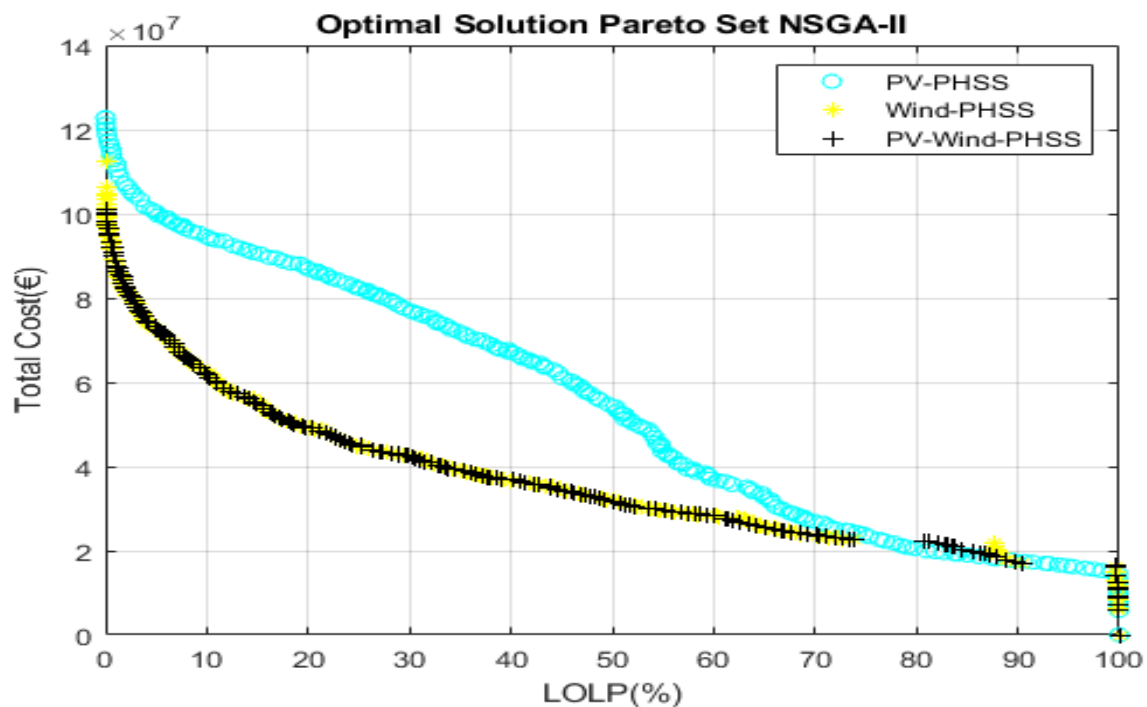**Figure 10.** Optimal pareto-front set OF NSWOA.

Figure 11. Optimal Pareto-front set of NSGA-II.

All numerical values are recorded from the output of NSWOA and NSGA-II in three different seniors, as shown in Table 2. Some of the outputs, such as total cost (€) and reservoir volume m³, are approximated by their decimal numerical values. Some are close to their decimal values for two or three digits to make them more accurate, including energy storage capacity (MWh), levelized cost of energy (LCOE) (€/kWh) for wind, PV, and PHS, and output power (MW) for wind and PV.

8.3. Comparison of the Results of the Two Algorithms

The obtained results, presented in Figures 10 and 11 and Table 2, show the Pareto-front obtained for the various scenarios studied thanks to the optimization techniques of NSWOA and NSGA-II. The total costs, at an LOLP equal to zero, thanks to the use of NSWOA are 121,760,835€, 105,596,880€, and 100,749,018€, respectively, for the PV-PHS, Wind-PHS, and PV-Wind-PHSS scenarios. As for the results obtained using the NSGA-II algorithm, at an LOLP equal to zero, the total costs of all systems are 122,814,628€ for the PV-PHSS scenario, 112,470,873€ for the Wind-PHSs scenario, and 100,969,133€ for the PV-Wind-PHSS scenario. The comparative analysis of the results provided by the two algorithms shows that the NSWOA algorithm gave better results than the NSGA-II algorithm. Indeed, the result obtained for the PV-PHSS scenario with the NSWOA algorithm is, in terms of total project cost, 1% lower than the total cost obtained for the same scenario with the NSGA-II. It is the same for the Wind-PHSs scenario, where NSWOA presents a 6% lower total cost than the one obtained with NSGA-II. As for the PV-Wind-PHSS scenario, the difference between the total cost obtained with NSWOA and the total cost obtained with NSGA-II is about 0.2%. Therefore, in this study, whose primary objective is to substitute diesel thermal power plants with renewable energy sources at a lower cost with a zero deficit, the NSWOA algorithm has delivered the best results for this optimization problem. The rest of the study will focus only on the NSWOA results.

The comparative study of the results of the different scenarios obtained with the NSWOA algorithm shows that with an LOLP equal to zero, the total cost of the PV-Wind-PHSS scenario is respectively 4.6% and 17% lower than the Wind-PHSS and PV-PHSS scenarios.

8.4. Analysis of the Results

Table 2 shows that the LCOEs for PV and wind systems are the same regardless of the scenarios considered. The LCOE of the PV system is 0.0422 €/kWh in both the PV-PHSS and PV-Wind-PHSS scenarios. The same is true for the wind system's LCOE, which is 0.025 €/kWh in both Wind-PHSS and PV-Wind-PHSS scenarios.

The LCOE of the PHS storage system, on the other hand, varies significantly depending on the scenario considered. For the PV-PHSS, Wind-PHSS, and PV-Wind-PHSS scenarios, it is 0.0604 €/kWh, 0.3851 €/kWh, and 0.2309 €/kWh, respectively. This significant variation in storage system LCOE across the scenarios considered can be explained by the low demand on the storage system in scenarios with wind power. In contrast to solar radiation, which disappears at night, wind can blow at any time of day. In the PV-PHSS scenario, the installed capacity is 35 MW, the daily energy storage capacity is 403.82 MWh/day, and the upper reservoir volume is 645,955.6 m^3.

The PHS system is requested in the Wind-PHSS scenario only when the available wind is insufficient to allow the wind turbines to provide the energy required to meet the demand. The algorithm selected 21.2303 MW as the optimal capacity for the PHS system, 204.34 MWh/day as the daily energy storage capacity, and 326,863.5 m^3 as the upper reservoir volume. The average wind speed is at its lowest during the rainy season, which lasts from April to October, as illustrated in Figures 3 and 6. As a result, in this scenario, the PHS storage system is really needed during this season.

Similarly, the PHS demand is low in the PV-Wind-PHSS scenario due to the presence of the wind system. The installed capacity of PHSS is 22.146 MW, the daily energy storage capacity is 191.71 MWh/day, and the upper reservoir has a capacity of 306,657.86 m^3.

Based on the data presented above, the LCOE, which is the ratio of the total lifetime cost of the system to the amount of energy the system can deliver, is higher for the PHS system in the Wind-PHSS and PV-Wind-PHSS scenarios than in the PV-PHSS scenario.

Figure 12 depicts the share of total project cost for each renewable energy system (RES) in each scenario. The PV system accounts for 60% of the total project cost in the PV-PHSS scenario, while the PHS system accounts for the remaining 40%. The wind system alone accounts for 75% of the total project cost in the Wind-PHSS scenario, with the PHSS system accounting for the remaining 25%. The wind system alone accounts for 56% of the total project cost in the PV-Wind-PHSS scenario, the PV system accounts for 18% of the expenses, and the PHS system accounts for 26% of the total project cost. The RES absorbs the majority of the expenses in all scenarios.
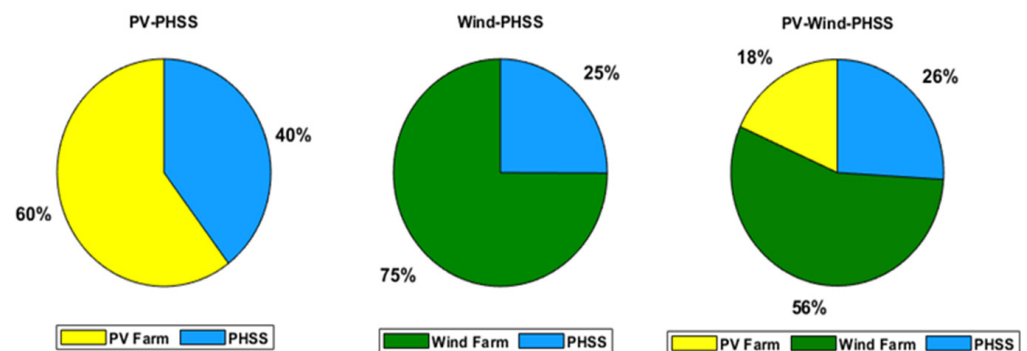

Figure 12. Share of each renewable energy system (RES) in the total project cost.

Figure 13 shows the results for an LOLP equal to zero of the PV, wind, and PHS outputs and the power flow on the grid over a period of one year obtained with NSWOA.

According to Figure 13, the PV field production in the PV-PHSS scenario ranges from 0 to 59.71 MW for an annual energy production of 135,174.92 MWh, of which 77,521.96 MWh is consumed by the PHS system to fill the upper water reservoir and 14,611.04 MWh is the surplus energy generated over a year. In this study scenario, the maximum power that can flow through the northern interconnected grid is 99.71 MW. The PHS system, which

has a capacity of 35 MW, consumes a large portion of this power. When the solar array meets all demand, the energy produced by the PHS system ranges from 0 MW to 22 MW, representing the maximum load demand. The amount of water consumed per hour by the PHS system varies inextricably with the amount of energy produced by the PHS system. Thus, the minimum amount of water consumed is none, and the maximum amount of water consumed is 35,191.8 m^3, which corresponds to the amount of water required to produce 22 MWh at 260 m altitude. Similarly, the amount of water pumped to fill the upper reservoir varies in tandem with the amount of energy consumed by the PHS system. It fluctuates between 0 and 41,990.04 m^3, corresponding to the maximum capacity of the PHS of 35 MW.

In the Wind-PHSS scenario, the wind farm produces between 902.58 kW and 42.30 MW for an annual energy output of 234,509.96 MWh, of which 6671.60 MWh is consumed by the PHS system to fill the upper reservoir with water and 131,533.27 MWh represents the surplus energy generated over a one-year period. When the hydroelectric dam is considered a base load and injects a constant power of 40 MW into the electrical grid, the maximum power that can flow on the northern interconnected grid in this study scenario is 82.3 MW. The PHS system uses a small portion of the energy generated by the wind system to fill the upper reservoir. In generation mode, the energy produced by the PHS system ranges from 0 MW when the wind field meets all demand to 21.04 MW when the wind field can only produce 996 kW. The amount of water consumed per hour by the PHS to generate power varies inextricably with the amount of energy produced by the PHS. Thus, the minimum amount of water consumed is none and the maximum amount of water consumed is 33,662.88 m^3, which corresponds to the amount of water required to produce 21.04 MWh at 260 m altitude. Similarly, the amount of water pumped to fill the upper reservoir varies in lockstep with the amount of energy consumed by the PHS system in pumping mode. It fluctuates between 0 and 24,214.32 m^3, corresponding to 20.183 MWh of consumed energy.
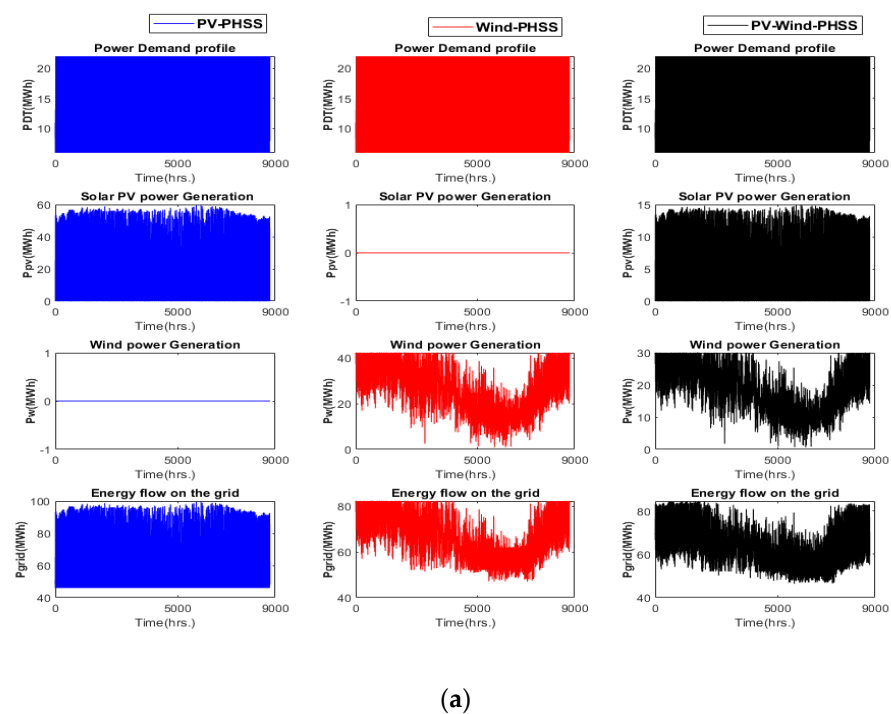

(a)

Figure 13. *Cont.*

(b)

(c)

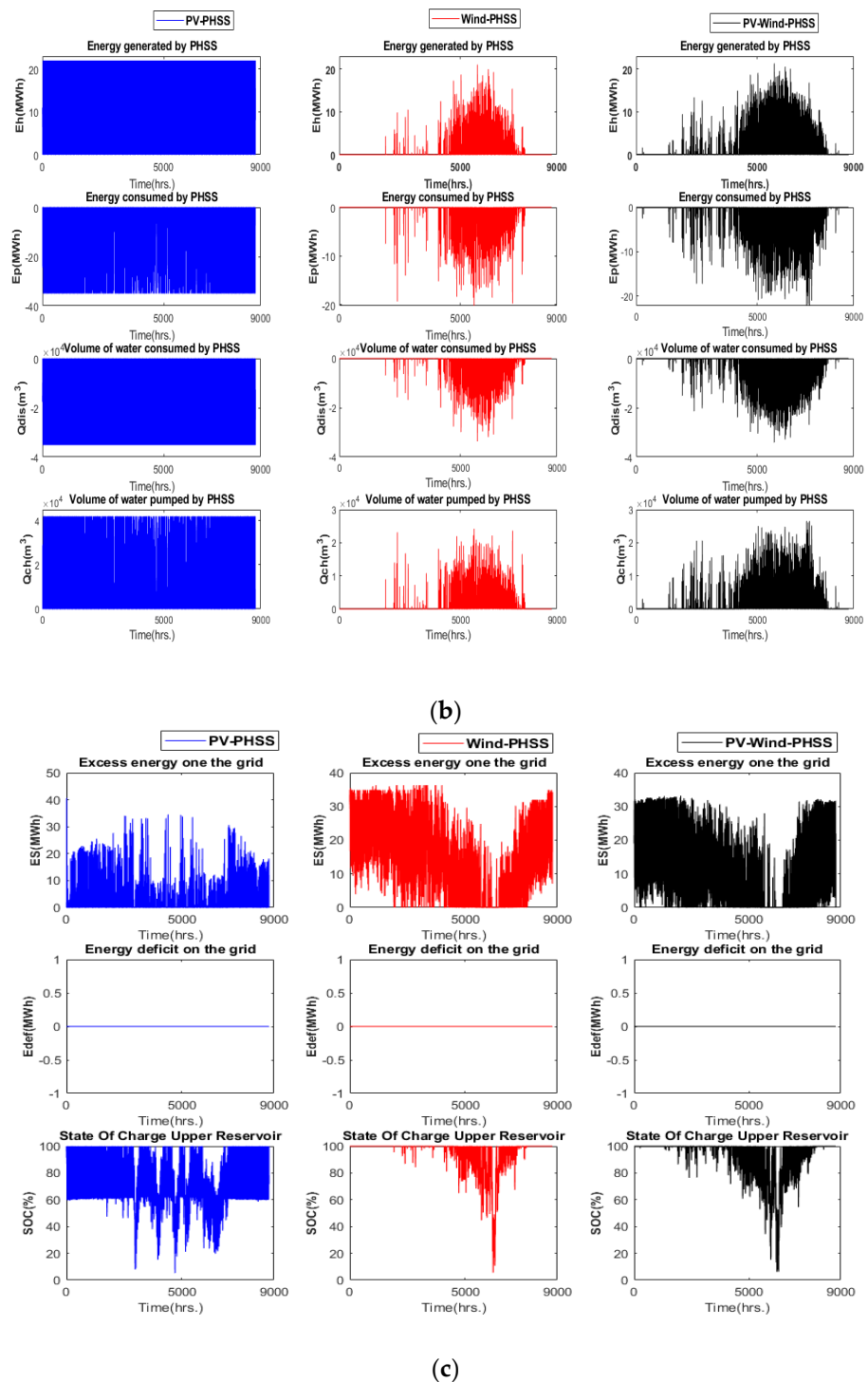**Figure 13.** (**a**–**c**) NSWOA algorithm results for the optimal solutions.

The wind field's output varies between 640.13 kW and 30 MW in the PV-Wind-PHSS scenario, for an annual energy generation of 166319.12 MWh. The solar photovoltaic farm's output ranges between 0 and 15.015 MW, for a total annual energy generation of 33,992.05 MWh. The total output of both energy sources ranges between 640.13 kW and 45.015 MW, for a total annual energy output of 200,311.17 MWh, of which 10,996.64 MWh is consumed by the PHS system to fill the upper water tank and 96253.36 MWh represents the surplus energy generated over a year. The maximum power flowing through the northern interconnected grid in this study scenario is 84.655 MW when the hydroelectric dam is considered a base load and provides 40 MW constantly into the grid. A small portion of the energy

generated by the wind system is consumed by the PHS system to fill the upper reservoir. The energy produced by the PHS system varies from 0 MW when the wind and PV fields meet all the demand to 21.322 MW. The amount of water consumed per hour by the PHS system to produce energy follows exactly the same variation as the energy generated by the PHS system. Thus, the minimum amount of water consumed is 0 and the maximum is 34,107.48 m^3, corresponding to the amount of water needed to produce 21.322 MWh at 260 m altitude. Similarly, the amount of water pumped to fill the upper reservoir varies in lockstep with the amount of energy consumed by the PHS system while pumping. It varies between 0 and 26,569.08 m^3, corresponding to 22.146 MW.

Figure 14 shows the proportions of useful energy in relation to the objective of replacing the thermal generation units by RES and the excess energy in the different scenarios studied. The excess energy in the PV-PHSS scenario is quite small and represents about 11% of the total energy generated by the PV field. The vast majority of the energy generated (about 57%) is consumed by the PHS system to fill the upper tank; the rest is directly consumed by the loads.
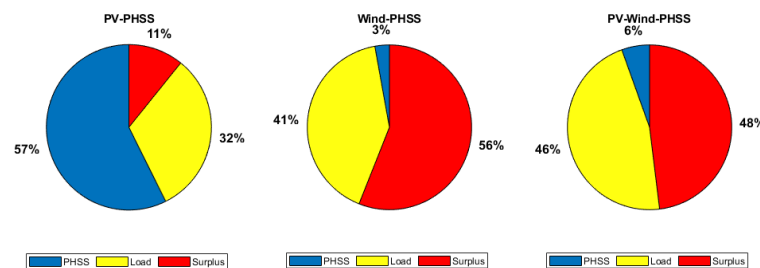

Figure 14. Share of the total energy generated by the RES in terms of the demand, the consumption of the PHS system and the surplus of energy.

In the Wind-PHSS scenario, the excess energy represents more than half of the energy produced by the wind field (about 56%). The energy consumed by the PHS system is very small and represents about 3% of the total energy generated by the wind system.

In the PV-Wind-PHSS scenario, the surplus energy represents 48% of the total energy generated by the PV and Wind fields. The energy consumed by the PHS system in pumping mode represents 6% of the total energy produced by the RES. The supply of energy to the different loads is done in a more deferred way in the PV-PHSS scenario and this explains in part, the very high solicitation of the storage system in this scenario. On the other hand, the energy consumption in the other two scenarios is much more direct between the generation systems and the loads.

As shown in Figure 15, the share of the PHS system in the energy delivered to the loads varies considerably between the scenarios considered. In the PV-PHS scenario, about 58% of the energy supplied to the loads is provided by the PHS system. On the other hand, the share of the PHS system in the energy delivered to the loads is low and around 5% in the Wind-PHSS scenario. In the PV-Wind-PHSS scenario, the PHS system only contributes about 8% of the annual load demand. In all scenarios, the remaining energy is supplied by renewable energy sources.
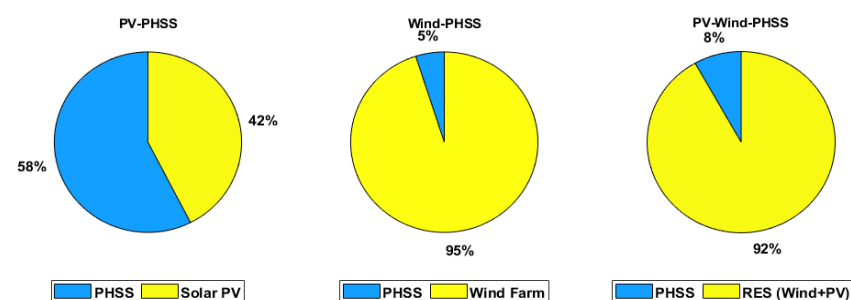

Figure 15. Role of storage in covering total energy demand for a 0% LOLP.

The project's cost-effectiveness study was done by considering all possible scenarios. At the level of each scenario, two major considerations have been made. The first was to evaluate the profitability of the whole project by considering the total energy demand for which the systems are designed. The second consideration was to see if eventually the surplus energy on the electrical network could be consumed by perhaps expanding the distribution network to new localities in northern Cameroon, and to observe the impact on the profitability of the system. The selling cost of the energy considered is 0.092 €/kWh. As shown in Figure 16, all three scenarios are profitable before the end of the 20 years of the project. However, the PV-Wind-PHSS scenario is quickly more profitable with a payback time of 14 years, while the Wind-PHSS scenario comes second with a payback time of 14 years, and finally the PV-PHSS scenario follows with a payback time of 19 years. In the case where excess energy is assumed to be sold in all scenarios, the payback time becomes shorter in the scenarios. In this case, the Wind-PHSS scenario becomes more profitable than the other two scenarios with a payback time of 5 years while the PV-Wind-PHSS scenario comes second and has a payback time of 6 years. Finally, the PV-PHSS scenario comes last with a payback time of 17 years. This change in trends between the different considerations can be explained by the higher energy surplus observed in the Wind-PHSS scenario. The consideration of the consumption of the excess energy by new loads remains hypothetical and is for comparison purposes only.
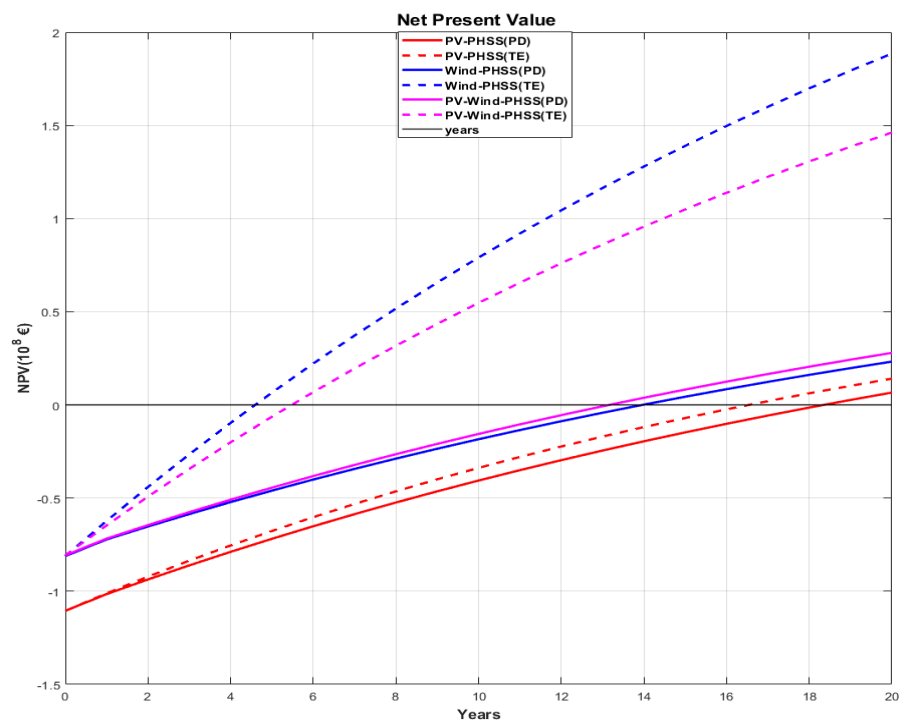

Figure 16. Net present values for all scenarios.

9. Conclusions

This work studied the different aspects of the substitution of thermal power plants connected to the interconnected grid of northern Cameroon by renewable energy plants. The optimization techniques used in this study for the optimal sizing of RES components are the NSWOA and NSGA-II algorithms. Different scenarios such as the PV-PHSS scenario, the Wind-PHSS scenario and the PV-Wind-PHSS scenario were studied in order to select the best one. The results obtained for the LOLP criterion equal to zero with the NSWOA algorithm gave, respectively, 121,760,835.144€, 105,596,880.427€ and 100,749,018.0955€ for the PV-PHSS, Wind-PHSS and PV-Wind-PHSS scenarios. As for the NSGA-II algorithm, the results obtained for the total cost of the project for an LOLP equal to zero are 122,814,628.757 € for the PV-PHSS scenario, 112,470,873.797€ for the Wind-PHSS scenario

and 100,969,133.109€ for the PV-Wind-PHSS scenario. The analysis of these results provided by the two algorithms revealed that the NSWOA algorithm provided better results than NSGA-II. The total cost in the PV-PHSS, Wind-PHSS, and PV-Wind-PHSS scenarios with NSWOA is, respectively, 1%, 6%, and 0.2% lower than in the NSGA-II. According to NSWOA results, the total cost for the PV-Wind-PHSS scenario at LOLP 0% is 4.6% and 17% less than the Wind-PHS and PV-PHSS scenarios, respectively. In addition, the PV-Wind-PHSS scenario has the lowest total project cost. Finally, the profitability study of the project in the three study scenarios showed that the project is profitable, whatever the scenario considered, before 20 years, representing the study period considered.

Author Contributions: Conceptualization, I.A., A.A., T.F.A., E.T. and B.K.; methodology, I.A., A.A., I.A., E.T. and B.K.; software, I.A. and T.F.A.; validation I.A., A.A., T.F.A., E.T. and B.K.; methodology, I.A.; formal analysis, I.A., A.A.; investigation, I.A. and T.F.A.; resources, I.A., A.A., T.F.A., E.T. and B.K.; methodology, I.A.; data curation, I.A., A.A., T.F.A., E.T. and B.K.; methodology, I.A.; writing—original draft preparation, I.A., A.A., T.F.A., E.T. and B.K.; methodology, I.A.; writing—review and editing, I.A., A.A., T.F.A., E.T., J.B.B., W.B.N. and B.K.; methodology, I.A.; visualization, I.A., A.A., T.F.A., E.T., J.B.B., W.B.N. and B.K.; methodology, I.A.; supervision, I.A., A.A., T.F.A., E.T. and B.K.; methodology, I.A.; project administration, I.A., A.A., T.F.A., E.T., B.K. and J.B.B.; methodology, I.A., A.A., T.F.A., E.T. and B.K. All authors have read and agreed to the published version of the manuscript.

Conflicts of Interest: The authors declare no conflict of interest.

Nomenclature

A	Solar PV panel area in m^2	P_P	PHS Power consumed in pumping mode
area	upper reservoir surface	PHS	Pumped hydro storage
$C_{initial}$	Initial capital cost	P_{PHS}	Output power of PHS in generating mode
C_{i-PV}	Solar PV panels capital cost	P_{PHSn}	PHS rating power rating
C_{i-Inv}	Inverters capital cost	P_{PHSn}^{min}	Lower limit of PHS power rating
C_{i-PHS}	PHS generation capital cost	P_{PHSn}^{max}	Upper limit of PHS power rating
C_{i-WT}	Wind turbine capital cost	P_{inv}	total power of inverters
C_S	PHS reservoir capital cost	$P_{peak-PV}$	Peak power solar fields
$C_{O\&M}$	Operation & Maintenance cost	P_{LD}	Power produced by the Lagdo dam
$C_{O\&M-Inv}$	Inverter O&M cost	P_{rated}	Rated power of Wind turbineT
$C_{O\&M-FPHS}$	PHS fixed O&M cost	P_{WT}	Wind turbine power output
$C_{O\&M-VPHS}$	PHS variable O&M cost	q_{ch}	Upper reservoir pumping/charging rate
$C_{O\&M-PV}$	Solar panels O&M cost	q_{dis}	Upper reservoir discharging rate
$C_{O\&M-WT}$	Wind turbine O&M cost	TC	total cost
$C_{replace}$	Replacement cost	$TLCC$	Total life cycle cost
C_{savage}	Savage cost	TC_{PHS}	total cost of PHS system
C_t	cash inflow-outflow difference	TC_{PV}	total cost of PV system
d	Nominal interest rate	TC_{WT}	total cost of wind system
E_B	Energy balance	T_a	Ambient temperature
E_C	Upper reservoir energy storage capacity	T_{cref}	photovoltaic cell reference temperature

$E_P(t)$	Energy consumed by PHS in pumping mode	V	Volume of water available at t
E_{PHS}	Energy generated by PHS in generating mode	$V(t-1)$	Volume of water available at t-1
f	Inflation rate	V_{min}	Minimum permissible level of water in the reservoir
H	the upper reservoir's water level in relation to the lower reservoir	V_{max}	Maximum level of water in the reservoir
$hadd$	Upper reservoir water level height	V_{nmin}	Lower limit of reservoir volume
ir	Real interest rate	V_{nmax}	Upper limit of reservoir volume
k	Annual discount factor	WT	Wind turbine
$G(t)$	hourly solar radiation in W/m^2	v	Wind velocity
$LOLP$	Loss of load probability	v_{ci}	Wind turbine's speed on
n	Project lifetime	v_{co}	Wind turbine's speed off
N_{Inv}	Number of inverters	v_r	Wind turbine's speed rated
N_{PV}	Number of solar PV panel	α	Hellman exponent
N_{PV}^{min}	Miniimum number of solar panels	β	Temperature coefficient (%/°C)
N_{PV}^{max}	Maximum number of solar panels	γ	Water self-discharge rate
N_{WT}	Number of wind turbine	g	Gravitational constant
N_{WT}^{min}	Minimum number of WT	ρ	Water density
N_{WT}^{max}	Maximum number of WT	η_{pv}	efficiency of the solar panel
NOCT	nominal operating cell temperature	η_r	reference efficiency of the solar panel
NPV	Net present value	η_{pc}	degradation factor
P_{grid}	Grid power flow	η_t	PHS generation system efficiency
P_{grid}^{max}	Grid's maximum power capacity	η_P	efficiency of the pumping system

References

1. IEA. Global Energy Review: CO$_2$ Emissions in 2021—Analysis. Available online: https://www.iea.org/reports/global-energy-review-co2-emissions-in-2021-2 (accessed on 16 November 2022).
2. Shafiee, S.; Topal, E. When will fossil fuel reserves be diminished? *Energy Policy* **2009**, *37*, 181–189. [CrossRef]
3. Lange, M. Renewable Energy and Water Resources. In *Climate Vulnerability*; Academic Press: Amsterdam, The Netherlands, 2013. [CrossRef]
4. IEA. Wind—Fuels & Technologies. Available online: https://www.iea.org/fuels-and-technologies/wind (accessed on 27 September 2022).
5. Advantages and Challenges of Wind Energy. Energy gov. Available online: https://www.energy.gov/eere/wind/advantages-and-challenges-wind-energy (accessed on 27 September 2022).
6. Hunt, J.D.; Zakeri, B.; Nascimento, A.; Brandão, R. Pumped Hydroelectric Storage. In *Storing Energy with Special Reference to Renewable Energy Sources*; Elsevier: Amsterdam, The Netherlands, 2022; pp. 37–65. [CrossRef]
7. Rehman, S.; Al-Hadhrami, L.M.; Alam, M.M. Pumped hydro energy storage system: A technological review. *Renew. Sustain. Energy Rev.* **2015**, *44*, 586–598. [CrossRef]
8. Katsaprakakis, D.A.; Dakanali, I.; Condaxakis, C.; Christakis, D.G. Comparing electricity storage technologies for small insular grids. *Appl. Energy* **2019**, *251*, 113332. [CrossRef]
9. Arnaoutakis, G.E.; Kefala, G.; Dakanali, E.; Katsaprakakis, D.A. Combined Operation of Wind-Pumped Hydro Storage Plant with a Concentrating Solar Power Plant for Insular Systems: A Case Study for the Island of Rhodes. *Energies* **2022**, *15*, 6822. [CrossRef]
10. Javed, M.S.; Ma, T.; Jurasz, J.; Amin, M.Y. Solar and wind power generation systems with pumped hydro storage: Review and future perspectives. *Renew. Energy* **2019**, *148*, 176–192. [CrossRef]
11. Hoffstaedt, J.; Truijen, D.; Fahlbeck, J.; Gans, L.; Qudaih, M.; Laguna, A.; De Kooning, J.; Stockman, K.; Nilsson, H.; Storli, P.-T.; et al. Low-head pumped hydro storage: A review of applicable technologies for design, grid integration, control and modelling. *Renew Sustain. Energy Rev.* **2022**, *158*, 112119. [CrossRef]
12. Stocks, M.; Stocks, R.; Lu, B.; Cheng, C.; Blakers, A. Global Atlas of Closed-Loop Pumped Hydro Energy Storage. *Joule* **2020**, *5*, 270–284. [CrossRef]
13. Akter, H.; Howlader, H.O.R.; Saber, A.Y.; Hemeida, A.M.; Takahashi, H.; Senjyu, T. Optimal Sizing and Operation of Microgrid in a Small Island Considering Advanced Direct Load Control and Low Carbon Emission. In Proceedings of the 2021 International Conference on Science & Contemporary Technologies (ICSCT), Danang, Vietnam, 3–5 April 2021; pp. 1–5. [CrossRef]
14. Fathy, A.; Kaaniche, K.; Alanazi, T.M. Recent Approach Based Social Spider Optimizer for Optimal Sizing of Hybrid PV/Wind/Battery/Diesel Integrated Microgrid in Aljouf Region. *IEEE Access* **2020**, *8*, 57630–57645. [CrossRef]
15. Sanajaoba, S. Optimal sizing of off-grid hybrid energy system based on minimum cost of energy and reliability criteria using firefly algorithm. *Sol. Energy* **2019**, *188*, 655–666. [CrossRef]

16. Alishavandi, A.M.; Moghaddas-Tafreshi, S.M. Optimal sizing of a multi-energy system using a multi-agent decentralized operation model considering private-ownership. *Sustain. Energy Technol. Assess.* **2022**, *49*, 101699. [CrossRef]

17. Ishraque, F.; Shezan, S.A.; Nur, J.N.; Islam, S. Optimal Sizing and Assessment of an Islanded Photovoltaic-Battery-Diesel Generator Microgrid Applicable to a Remote School of Bangladesh. *Eng. Rep.* **2021**, *3*, 12281. [CrossRef]

18. Al-Masri, H.M.; Magableh, S.K.; Abuelrub, A.; Alzaareer, K. Realistic coordination and sizing of a solar array combined with pumped hydro storage system. *J. Energy Storage* **2021**, *41*, 102915. [CrossRef]

19. Nguyen, H.T.; Safder, U.; Nguyen, X.N.; Yoo, C. Multi-objective decision-making and optimal sizing of a hybrid renewable energy system to meet the dynamic energy demands of a wastewater treatment plant. *Energy* **2020**, *191*, 116570. [CrossRef]

20. Moghaddam, M.J.H.; Kalam, A.; Nowdeh, S.A.; Ahmadi, A.; Babanezhad, M.; Saha, S. Optimal sizing and energy management of stand-alone hybrid photovoltaic/wind system based on hydrogen storage considering LOEE and LOLE reliability indices using flower pollination algorithm. *Renew. Energy* **2019**, *135*, 1412–1434. [CrossRef]

21. Guo, S.; Kurban, A.; He, Y.; Wu, F.; Pei, H.; Song, G. Multi-objective sizing of solar-wind-hydro hybrid power system with doubled energy storages under optimal coordinated operation strategy. *CSEE J. Power Energy Syst.* **2021**, 1–11. [CrossRef]

22. Bhardwaj, H.; Saini, D.; Paliwal, N.; Mathur, A. Sizing Optimization of a Stand-Alone PV/Wind Power Supply System with Hybrid Energy Storage. In Proceedings of the 2022 IEEE Delhi Section Conference (DELCON), New Delhi, India, 11–13 February 2022; pp. 1–6. [CrossRef]

23. Alturki, F.A.; Awwad, E.M. Sizing and Cost Minimization of Standalone Hybrid WT/PV/Biomass/Pump-Hydro Storage-Based Energy Systems. *Energies* **2021**, *14*, 489. [CrossRef]

24. Makhdoomi, S.; Askarzadeh, A. Optimizing operation of a photovoltaic/diesel generator hybrid energy system with pumped hydro storage by a modified crow search algorithm. *J. Energy Storage* **2019**, *27*, 101040. [CrossRef]

25. Das, M.; Singh, M.A.K.; Biswas, A. Techno-economic optimization of an off-grid hybrid renewable energy system using metaheuristic optimization approaches—Case of a radio transmitter station in India. *Energy Convers. Manag.* **2019**, *185*, 339–352. [CrossRef]

26. Yang, D.; Zhu, T.; Wang, S.; Wang, S.; Xiong, Z. LFRSNet: A robust light field semantic segmentation network combining contextual and geometric features. *Front. Environ. Sci.* **2022**, *10*, 1443. [CrossRef]

27. Wang, Y.; Wen, X.; Gu, B.; Gao, F. Power Scheduling Optimization Method of Wind-Hydrogen Integrated Energy System Based on the Improved AUKF Algorithm. *Mathematics* **2022**, *10*, 4207. [CrossRef]

28. Xu, S.; Huang, W.; Wang, H.; Zheng, W.; Wang, J.; Chai, Y.; Ma, M. A Simultaneous Diagnosis Method for Power Switch and Current Sensor Faults in Grid-Connected Three-Level NPC Inverters. *IEEE Trans. Power Electron.* **2022**, *38*, 1104–1118. [CrossRef]

29. Zhang, W.; Zheng, Z.; Liu, H. A novel droop control method to achieve maximum power output of photovoltaic for parallel inverter system. *CSEE J. Power Energy Syst.* **2021**, *8*, 1636–1645. [CrossRef]

30. Wang, P.; Yu, P.; Huang, L.; Zhang, Y. An integrated technical, economic, and environmental framework for evaluating the rooftop photovoltaic potential of old residential buildings. *J. Environ. Manag.* **2022**, *317*, 115296. [CrossRef] [PubMed]

31. Diab, A.A.Z.; Sultan, H.M.; Kuznetsov, O.N. Optimal sizing of hybrid solar/wind/hydroelectric pumped storage energy system in Egypt based on different meta-heuristic techniques. *Environ. Sci. Pollut. Res.* **2019**, *27*, 32318–32340. [CrossRef]

32. Guezgouz, M.; Jurasz, J.; Bekkouche, B.; Ma, T.; Javed, M.S.; Kies, A. Optimal hybrid pumped hydro-battery storage scheme for off-grid renewable energy systems. *Energy Convers. Manag.* **2019**, *199*, 112046. [CrossRef]

33. Xu, X.; Hu, W.; Cao, D.; Huang, Q.; Chen, C.; Chen, Z. Optimized sizing of a standalone PV-wind-hydropower station with pumped-storage installation hybrid energy system. *Renew. Energy* **2019**, *147*, 1418–1431. [CrossRef]

34. Nyeche, E.; Diemuodeke, E. Modelling and optimisation of a hybrid PV-wind turbine-pumped hydro storage energy system for mini-grid application in coastline communities. *J. Clean. Prod.* **2019**, *250*, 119578. [CrossRef]

35. Rodrigues, S.; Bauer, P.; Bosman, P.A. Multi-objective optimization of wind farm layouts—Complexity, constraint handling and scalability. *Renew. Sustain. Energy Rev.* **2016**, *65*, 587–609. [CrossRef]

36. Jiang, H.; Liu, B.; Wang, Y.; Zheng, S. Multiobjective TOU Pricing Optimization Based on NSGAJ. *Appl. Math.* **2014**, *2014*, 104518. [CrossRef]

37. Ruiming, F. Multi-objective optimized operation of integrated energy system with hydrogen storage. *Int. J. Hydrogen Energy* **2019**, *44*, 29409–29417. [CrossRef]

38. Kamjoo, A.; Maheri, A.; Dizqah, A.M.; Putrus, G.A. Multi-objective design under uncertainties of hybrid renewable energy system using NSGA-II and chance constrained programming. *Int. J. Electr. Power Energy Syst.* **2016**, *74*, 187–194. [CrossRef]

39. Mukoni, E.; Garner, K.S. Multi-Objective Non-Dominated Sorting Genetic Algorithm Optimization for Optimal Hybrid (Wind and Grid)-Hydrogen Energy System Modelling. *Energies* **2022**, *15*, 7079. [CrossRef]

40. Kidmo, D.K.; Deli, K.; Bogno, B. Status of renewable energy in Cameroon. Renew. *Energy Environ. Sustain.* **2021**, *6*, 2. [CrossRef]

41. Solar Resource Maps of Cameroon. Available online: https://solargis.com/maps-and-gis-data/download/cameroon (accessed on 27 September 2022).

42. Estimating the Renewable Energy Potential in Africa: A GIS-Based Approach. Available online: https://www.irena.org/publications/2014/Aug/Estimating-the-Renewable-Energy-Potential-in-Africa-A-GIS-based-approach (accessed on 12 September 2022).

43. Bhusal, N.; Gautam, M.; Benidris, M.; Louis, S.J. Optimal Sizing and Siting of Multi-purpose Utility-scale Shared Energy Storage Systems. In Proceedings of the 2020 52nd North American Power Symposium (NAPS), Tempe, AZ, USA, 11–13 April 2021; pp. 1–6. [CrossRef]

44. Vukadinović, A.; Radosavljević, J.; Đorđević, A.; Protić, M.; Petrović, N. Multi-objective optimization of energy performance for a detached residential building with a sunspace using the NSGA-II genetic algorithm. *Sol. Energy* **2021**, *224*, 1426–1444. [CrossRef]

45. Islam, Q.N.U.; Ahmed, A.; Abdullah, S.M. Optimized controller design for islanded microgrid using non-dominated sorting whale optimization algorithm (NSWOA). *Ain Shams Eng. J.* **2021**, *12*, 3677–3689. [CrossRef]

46. Yin, X.; Cheng, L.; Wang, X.; Lu, J.; Qin, H. Optimization for Hydro-Photovoltaic-Wind Power Generation System Based on Modified Version of Multi-Objective Whale Optimization Algorithm. *Energy Procedia* **2019**, *158*, 6208–6216. [CrossRef]

47. Toro, S.M. Post-construction effects of the Cameroonian Lagdo dam on the River Benue. *Water Environ. J.* **1997**, *11*, 109–113. [CrossRef]

48. Grijsen, J.; Patel, H. Understanding the Impact of Climate Change on Hydropower: The Case of Cameroon—Climate Risk Assessment for Hydropower Generation in Cameroon, World Bank Group. 2014. Available online: https://policycommons.net/artifacts/1527630/understanding-the-impact-of-climate-change-on-hydropower/2216658/ (accessed on 16 November 2022).

49. Eneo2020AnnualReport.pdf. Available online: https://eneocameroon.cm/pdf/Eneo2020AnnualReport.pdf (accessed on 20 July 2022).

50. CAMS Radiation Service—SoDa. Available online: https://www.soda-pro.com/web-services/radiation/cams-radiation-service (accessed on 22 July 2022).

51. Kidmo, D.K.; Deli, K.; Raidandi, D.; Yamigno, S.D. Wind Energy for Electricity Generation in the Far North Region of Cameroon. *Energy Procedia* **2016**, *93*, 66–73. [CrossRef]

52. HOME—SoDa. Available online: https://www.soda-pro.com/ (accessed on 2 October 2022).

53. Nzotcha, U. Promoting Pumped Hydroelectric Energy Storage for Sustainable Power Generation in Cameroon: An Assessment of Local Opportunities. Ph.D. Thesis, Université de Yaoundé I, Yaoundé, Cameroon, 2020.

54. Available online: https://www.google.com/maps/place/Lac+Lagdo/@9.0547092,13.7284447,8219m/data=!3m1!1e3!4m5!3m4!1s0x10e4a099c18905ad:0x4aae22c8e99e5bd9!8m2!3d8.8738844!4d13.8332193 (accessed on 16 November 2022).

55. Belmili, H.; Haddadi, M.; Bacha, S.; Almi, M.F.; Bendib, B. Sizing stand-alone photovoltaic–wind hybrid system: Techno-economic analysis and optimization. Renew. Sustain. *Energy Rev.* **2014**, *30*, 821–832. [CrossRef]

56. Diaf, S.; Belhamel, M.; Haddadi, M.; Louche, A. Technical and economic assessment of hybrid photovoltaic/wind system with battery storage in Corsica island. *Energy Policy* **2008**, *36*, 743–754. [CrossRef]

57. Akram, U.; Khalid, M.; Shafiq, S. An Innovative Hybrid Wind-Solar and Battery-Supercapacitor Microgrid System—Development and Optimization. *IEEE Access* **2017**, *5*, 25897–25912. [CrossRef]

58. Aykut, E.; Terzi, K. Techno-economic and environmental analysis of grid connected hybrid wind/photovoltaic/biomass system for Marmara University Goztepe campus. *Int. J. Green Energy* **2020**, *17*, 1036–1043. [CrossRef]

59. Yimen, N.; Tchotang, T.; Kanmogne, A.; Idriss, I.A.; Musa, B.; Aliyu, A.; Okonkwo, E.; Abba, S.; Tata, D.; Meva'A, L.; et al. Optimal Sizing and Techno-Economic Analysis of Hybrid Renewable Energy Systems—A Case Study of a Photovoltaic/Wind/Battery/Diesel System in Fanisau, Northern Nigeria. *Processes* **2020**, *8*, 1381. [CrossRef]

60. Kusakana, K. Feasibility analysis of river off-grid hydrokinetic systems with pumped hydro storage in rural applications. *Energy Convers. Manag.* **2015**, *96*, 352–362. [CrossRef]

61. Das, P.; Das, B.K.; Mustafi, N.N.; Sakir, T. A review on pump-hydro storage for renewable and hybrid energy systems applications. *Energy Storag.* **2020**, *3*, e223. [CrossRef]

62. Renewable Power Generation Costs in 2021. Available online: https://irena.org/publications/2022/Jul/Renewable-Power-Generation-Costs-in-2021 (accessed on 4 October 2022).

63. Zakeri, B.; Syri, S. Electrical energy storage systems: A comparative life cycle cost analysis. *Renew. Sustain. Energy Rev.* **2015**, *42*, 569–596. [CrossRef]

64. GW 2S-Smart Wind Turbine | GOLDWIND Wind Turbine Manufacturer. Available online: https://www.goldwind.com/en/windpower/product-gw2s/ (accessed on 2 October 2022).

65. SMA America Confirms 25-Year Design Life for Sunny Highpower PEAK3 Inverters | SMA America. Available online: https://www.sma-america.com/newsroom/news-details/sma-america-confirms-25-year-design-life-for-sunny-highpower-peak3-inverters (accessed on 14 September 2022).

66. Kazem, H.A.; Albadi, M.; Al-Waeli, A.H.; Al-Busaidi, A.H.; Chaichan, M.T. Techno-economic feasibility analysis of 1 MW photovoltaic grid connected system in Oman. Case Stud. *Therm. Eng.* **2017**, *10*, 131–141. [CrossRef]

67. Ndwali, K.; Njiri, J.G.; Wanjiru, E.M. Multi-objective optimal sizing of grid connected photovoltaic batteryless system minimizing the total life cycle cost and the grid energy. *Renew. Energy* **2019**, *148*, 1256–1265. [CrossRef]

68. Arabi-Nowdeh, S.; Nasri, S.; Saftjani, P.B.; Naderipour, A.; Abdul-Malek, Z.; Kamyab, H.; Jafar-Nowdeh, A. Multi-criteria optimal design of hybrid clean energy system with battery storage considering off- and on-grid application. *J. Clean. Prod.* **2021**, *290*, 125808. [CrossRef]

69. Gharavi, H.; Ardehali, M.; Ghanbari-Tichi, S. Imperial competitive algorithm optimization of fuzzy multi-objective design of a hybrid green power system with considerations for economics, reliability, and environmental emissions. *Renew. Energy* **2015**, *78*, 427–437. [CrossRef]

70. Bruck, M.; Sandborn, P.; Goudarzis, N. A Levelized Cost of Energy (LCOE) model for wind farms that include Power Purchase Agreements (PPAs). *Renew. Energy* **2018**, *122*, 131–139. [CrossRef]

71. Bruck, M.; Sandborn, P. Pricing bundled renewable energy credits using a modified LCOE for power purchase agreements. *Renew. Energy* **2021**, *170*, 224–235. [CrossRef]

72. Yang, S.; Zhu, X.; Guo, W. Cost-Benefit Analysis for the Concentrated Solar Power in China. *J. Electr. Comput. Eng.* **2018**, *2018*, 4063691. [CrossRef]

73. Deb, K.; Agrawal, S.; Pratap, A.; Meyarivan, T. A Fast Elitist Non-dominated Sorting Genetic Algorithm for Multi-objective Optimization: NSGA-II. In *International Conference on Parallel Problem Solving from Nature*; Springer: Berlin, Germany, 2000; pp. 849–858. [CrossRef]

74. Mirjalili, S.; Lewis, A. The Whale Optimization Algorithm. *Adv. Eng. Softw.* **2016**, *95*, 51–67. [CrossRef]

75. RESEARCH—SoDa. Available online: https://www.soda-pro.com/research-projects (accessed on 16 November 2022).